6 Magnetic confinement fusion: tokamak

[D. Campbell]

6.1 Introduction

Development of plasma parameters required for fusion power production is most advanced in the tokamak, the most successful of the toroidal magnetic confinement systems explored during the last 50 years of controlled fusion research. Fundamental principles of this concept were developed initially in the former Soviet Union during the 1950s and the name derives from the Russian words *toroidalnaya kamera* and *magnitnaya katushka*, meaning "toroidal chamber" and "magnetic coil". The major stimulus for the concentration on tokamak research within the magnetic fusion program was the announcement in 1968, by a group at the Kurchatov Institute in Moscow, that plasmas in the T-3 tokamak had reached the then unheard of temperature of 1 keV (1 keV = 1.16×10^7 K is the conventional unit of temperature in fusion research) [69P1].

The essential principle of the tokamak configuration can be understood by considering that a long straight solenoid is bent into a circle to form a *toroidal* magnet. Since the ions and electrons within the plasma are constrained to spiral around the magnetic field lines, they can, in principle, be confined by this toroidal magnetic field, B_ϕ, whose magnitude within the region defined by the coil winding is

$$B_\phi = \frac{\mu_0 I_\phi}{2\pi R} \ , \tag{6.1}$$

where I_ϕ is the total current flowing in the coil and R the distance from the axis of the torus (Fig. 6.1a). However, the toroidal magnetic field is curved and, as demonstrated by (6.1), its magnitude decreases with increasing radius from the torus center. Both of these effects distort the gyro-orbits of the particles and cause them to drift up or down across the field lines. Ions and electrons drift in opposite directions, causing an electric field to develop and further enhancing the loss of plasma across the field lines. As shown in Fig. 6.1a, a *poloidal* magnetic field, which acts at right angles to the toroidal field, can be added. The poloidal field is produced by a toroidal current flowing in the plasma which is induced via transformer coupling between a vertical solenoid, wound inside the central hole of the torus, and the toroidal ring of plasma.

The resultant magnetic field consists of a set of nested helical field lines and, as the particles follow these helical trajectories around the torus, the drifts are canceled, producing a well confined magnetoplasma. Figure 6.1a defines the basic geometry of the tokamak configuration, while Fig. 6.1b illustrates the spatial variation and magnitude of the toroidal and poloidal magnetic fields across the poloidal cross-section of the torus in a typical large tokamak. Additional poloidal field components can be applied by external coils to shape the plasma cross-section and to control its position. The main elements of a large tokamak, the Joint European Torus (JET), are illustrated in Fig. 6.2.

To attain the necessary conditions for fusion power production the plasma must be heated to a sufficiently high temperature at adequate densities so that the deuterium and tritium nuclei react, producing energy in the form of helium nuclei (α-particles) and neutrons. 80 % of the kinetic energy released by the reactions is carried away by the neutrons, which are immediately lost from the plasma and are absorbed in the structure of the chamber, providing most of the energy for steam generation in a power plant. Therefore, to achieve a positive energy balance within the plasma, the energy of the α-particles must be efficiently transferred to the plasma particles and used to maintain the high temperature and density. This requirement is summarized in the concept of energy confinement time, τ_E,

$$\tau_E = \frac{W_{\text{th}}}{P_{\text{loss}}} \ , \tag{6.2}$$

where W_{th} is the thermal energy of the plasma particles and P_{loss} the power lost from the plasma by all energy transport processes. To achieve "ignition", where the power transferred from the α-particles to the plasma just balances P_{loss}, the plasma must be maintained at a temperature of approximately 10 keV (nearly a factor of 10 greater than at the center of the sun) at a particle density in the region of 10^{20} m^{-3} (about 10^{-6} of the density of air), with an energy confinement time of about 5 s.

The physical concepts associated with establishing the magnetic configuration in a tokamak and raising the plasma temperature and density are dealt with in Sects. 6.2 and 6.3. The processes which lead to energy loss from the plasma and the resultant characteristics of energy and particle confinement are discussed in Sect. 6.4, while the principal forms of plasma instability are reviewed in Sect. 6.5, and the problems and achievements in the area of power and particle exhaust are considered in Sect. 6.6. Requirements for steady-state operation of tokamaks, together with relevant experimental results, are reviewed in Sect. 6.7, and physics issues associated with energetic particle populations, i.e. particle populations with characteristic energies many times that of the plasma temperature, are addressed in Sect. 6.8. The principal achievements of contemporary tokamak experiments and the major developments which are underway are reviewed in Sect. 6.9. These devices have provided the physics and technical bases for a tokamak burning plasma experiment which would demonstrate substantial fusion power production, several hundred MW, for hundreds of seconds and which would integrate many key aspects of the technology required for the core of a fusion power plant. The design and predicted performance of this device, known as the International Thermonuclear Experimental Reactor, are summarized in Sect. 6.10, where the principal characteristics of a tokamak fusion power plant are also discussed.

The presentation in this chapter is necessarily concise. More detailed discussions of the physics of tokamak plasmas can be found in [92K1] and [97W1], while [99I1] presents a contemporary review of the status of experimental and theoretical understanding of tokamak plasmas, and [94S1] discusses the physics of magnetically confined plasmas in a reactor context.

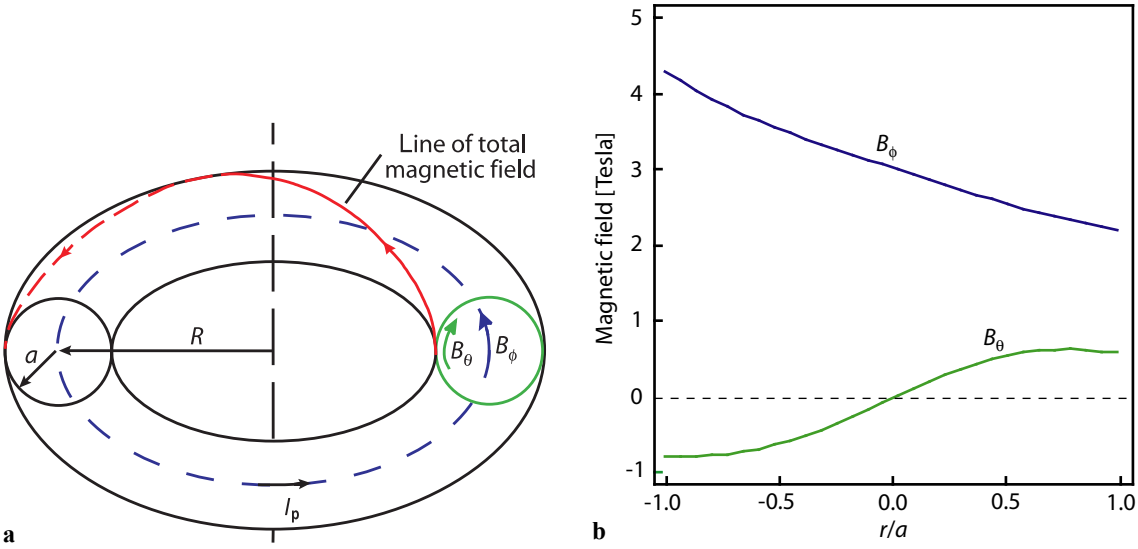

Fig. 6.1. **(a)** Schematic of the tokamak magnetic field geometry illustrating the principal parameters. The distance from the central axis of symmetry to the center of the toroidal ring is the major radius, R, the distance from the center of the toroidal ring to its edge is the minor radius, a, and the ratio R/a is the "aspect ratio". The toroidal field, B_ϕ, is directed around the long circumference of the torus, while the poloidal field, B_θ, is directed around the short circumference. The field line corresponding to the total field then forms a helix around the torus and the magnetic configuration consists of a set of nested helices with different pitch angles. **(b)** Spatial variation of the toroidal and poloidal fields across the poloidal cross-section of the torus in a tokamak (r is the minor radius coordinate). Note the difference in magnitude of the two.

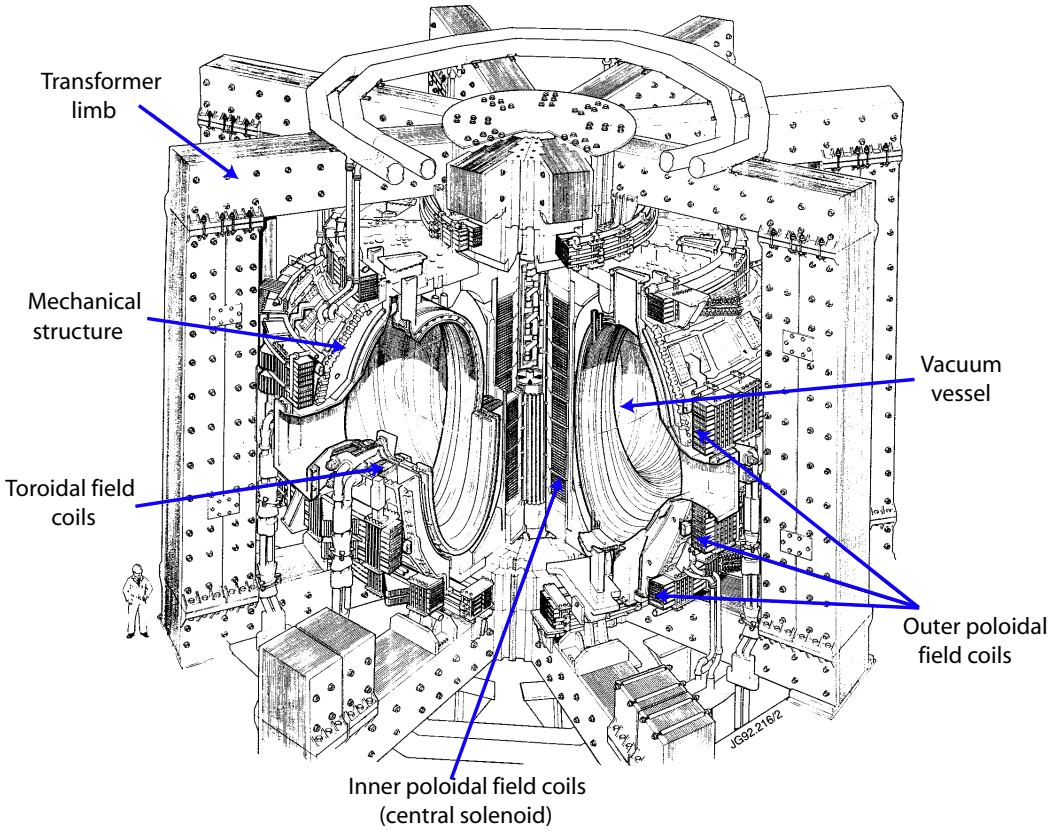

Fig. 6.2. Schematic of the JET tokamak, showing the main elements of the magnetic coil configuration and of the mechanical structure. The iron transformer is an optional component in the poloidal field circuit of the tokamak which improves the inductive coupling between the solenoid (primary winding in the figure) and the plasma current ring, and reduces stray magnetic fields.

6.2 The tokamak configuration

6.2.1 Tokamak equilibrium

The concept of "equilibrium" in magnetically confined plasmas refers both to the existence of force balance between the magnetic and kinetic forces within the plasma, and to the plasma position and shape as determined by the interaction between the plasma current distribution and the fields produced by the external coil systems (e.g. [66S1, 89M1, 97W1]).The former condition requires that the force on the plasma is zero at all points and, in the simplest approximation where fluid flows are neglected, that the magnetic force balances that due to the plasma pressure, a condition which can be expressed as

$$\boldsymbol{j}\times\boldsymbol{B}=\nabla p \ , \tag{6.3}$$

where $\boldsymbol{j}$ is the local current density, $\boldsymbol{B}$ the total magnetic field and p the plasma pressure. In an axisymmetric equilibrium, in which the equilibrium is independent of the toroidal angle, ϕ, the magnetic field lines form nested toroidal surfaces which can be identified with a poloidal magnetic flux function, ψ, which is constant on a magnetic surface. Equation (6.3) then has far-reaching consequences for plasma properties. In particular, it implies that the plasma pressure, and hence the density and temperature, is constant within each magnetic surface and that the lines of plasma current also lie within the magnetic

surfaces. There is therefore a strong degree of symmetry within tokamak plasmas and, in many cases of interest, the only significant gradients in density and temperature are normal to the nested flux surfaces.

In Fig. 6.1a, the tokamak plasma is shown in a simplified form as a torus of circular cross-section, but in many modern tokamak experiments the plasma equilibrium is elongated vertically, the poloidal cross-section is made triangular, and the magnetic field lines at the plasma edge form a poloidal null or X-point, i.e. a region in which the poloidal field is zero, a configuration which allows improved control of the plasma-wall interaction (discussed in Sect. 6.6). These aspects are illustrated in Fig. 6.3, which shows a poloidal cross-section of the plasma equilibrium in the Axisymmetric Divertor Experiment (ASDEX) Upgrade tokamak, located in Germany. The plasma elongation, κ, is defined by

$$\kappa = \frac{b}{a} \ , \tag{6.4a}$$

where b is the minor radius of the plasma in the vertical direction and a the minor radius in the horizontal direction, and the plasma triangularity, δ, is defined in a simple approximation as

$$\delta = \frac{R_0 - R_D}{a} \ , \tag{6.4b}$$

where R_0 is the major radius of the toroidal line corresponding to the center of the magnetic flux surfaces and R_D is the major radius at which the vertical minor radius is measured. In current tokamaks, the elongation typically lies in the range $1 \leq \kappa \leq 2$ and the triangularity in the range $0 \leq \delta \leq 1$.

The more complex equilibria exemplified by Fig. 6.3 are obtained by using additional external coil sets, such as those illustrated in the figure, to deform the plasma into the required shape via magnetostatic attraction and repulsion. The external coil sets must also provide active positional control for the plasma since both the radial and vertical positions are intrinsically unstable. Radial position control is required since the toroidal geometry produces a hoop force which tends to expand the plasma ring and which must be counteracted by a vertical field, whose magnitude depends on the magnitude and internal distribution of the plasma current, the plasma pressure, and plasma geometric parameters. Plasmas with $\kappa > 1$ are unstable against vertical displacements (see Sect. 6.5.2) and the plasma vertical position must be actively maintained by a combination of poloidal field coils which imposes a time-varying radial field in response to vertical motions of the plasma.

The poloidal field coils in a tokamak therefore serve three functions: by transformer action they provide the electric field required to produce the plasma ("breakdown") and to drive the plasma current; they shape the plasma and, if necessary, produce an X-point at the boundary; and they maintain the plasma radial and vertical positions under active feedback control.

For the plasma illustrated in Fig. 6.3, the region of good plasma confinement, in which the magnetic flux surfaces are "closed", is defined by the flux surface which forms an X-point. Outside of this special surface, known as a magnetic separatrix, the flux surfaces are "open", i.e. they intersect the chamber wall at some point. Particles which cross the separatrix from the main plasma to the open field lines, flow along the field lines and intersect the divertor target at the bottom of the vacuum vessel in the figure. There are two generic X-point configurations: the single null X-point (SNX) plasma, having a single field null in the separatrix, at either the top or bottom of the plasma, and the double null X-point (DNX) plasma, having field nulls at both top and bottom. There are many detailed differences in plasma behavior between single and double null X-point plasmas, and the choice of a preferred configuration depends largely on which of these differences is emphasized.

An alternative approach to the definition of the plasma boundary, and to the control of interactions between the plasma and the chamber wall, is the use of a "limiter". This involves a specially prepared surface which intersects the helical field lines just inside the bore of the vacuum chamber and which "scrapes off" particles traveling on these field lines. In this case, the plasma boundary is referred to as the "last closed flux surface" (LCFS), a term which can also be applied to the magnetic separatrix.

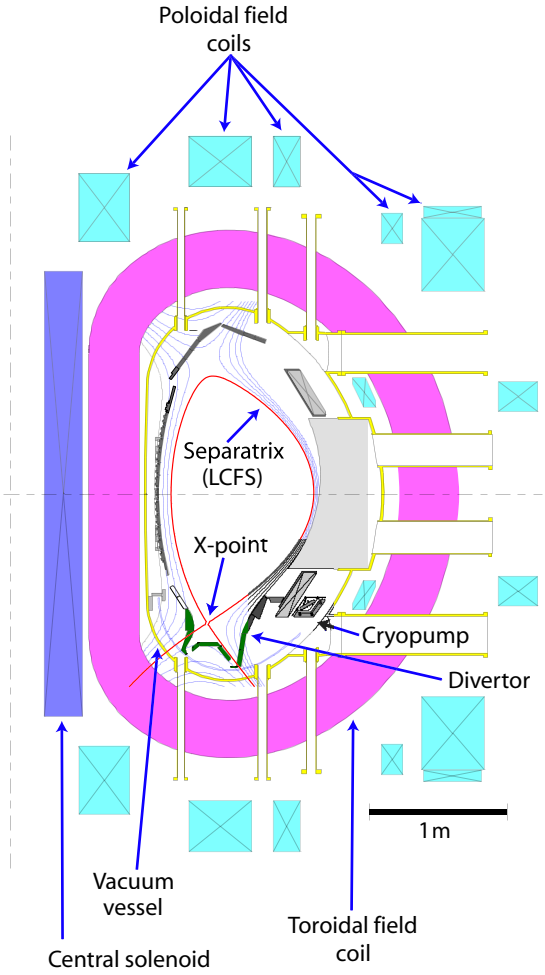

Fig. 6.3. Poloidal cross-section of the ASDEX Upgrade tokamak, showing the main elements of the poloidal coil configuration, together with a highly shaped plasma equilibrium, which is both elongated and triangular. At the plasma edge, the "last closed flux surface" (LCFS) forms an "X-point" in the lower region of the figure and below this the magnetic surfaces are formed into a "diverted" configuration.

6.2.2 Plasma equilibrium parameters

Several parameters are used to characterize the major features of the plasma equilibrium. The safety factor, q, describes the nature of the helical field and is most simply thought of as a "magnetic winding number" which gives the number of times that a helical field line must circle the torus toroidally before it returns to the same place in the poloidal plane. Formally, it is defined for any magnetic surface as the local rate of change of toroidal flux, Φ, with poloidal flux, Ψ, at the surface in question,

$$q = \frac{\mathrm{d}\Phi}{\mathrm{d}\Psi} \ . \tag{6.5}$$

For a plasma of circular poloidal cross-section and large aspect ratio ($R/r >> 1$), it can be approximated as

$$q_\mathrm{c}(r) = \frac{rB_\phi}{R_0 B_\theta(r)} \ , \tag{6.6}$$

where $q_\mathrm{c}(r)$ is the "cylindrical safety factor" and r is the minor radius of an arbitrary point inside the plasma. In highly shaped plasmas, the elongation and triangularity also play a role, and at lower aspect ratio toroidicity causes an additional deviation from the simple form of (6.6). In magnetic separatrix plasmas, the low value of the poloidal field in the vicinity of the X-point causes q to approach infinity as the separatrix is approached. A convention has therefore developed in which the edge safety factor of mag-

netic separatrix plasmas is defined in terms of the q-value at the flux surface which includes 95 % of the poloidal flux in the plasma, written q_{95}. Various approximations exist for this quantity (e.g. [91P1, 93T1]), depending on the degree to which geometric and other equilibrium parameters are considered. A form which depends only on geometric parameters [91P1] is:

$$q_{95} = \frac{2.5\,a^2 B_\phi [1+\kappa^2(1+2\delta^2-1.2\delta^3)][1.17-0.65\varepsilon]}{R I_\mathrm{p}[1-\varepsilon^2]^2} \ , \tag{6.7}$$

where I_p is the plasma current and $\varepsilon = a/R_0$ is the inverse aspect ratio.

The absolute value of q and its variation across the plasma cross-section have important consequences for the growth of instabilities in the plasma ring, since these often develop around surfaces having $q = m/n$, where m and n are integers (see Sect. 6.5). Usually, though not invariably, q is a minimum in the plasma center, with a value of order unity, and it rises monotonically towards the plasma edge, where values of 3…5 are typical (for a magnetic separatrix plasma, this would correspond to q_{95}). The variation of q across the plasma minor radius is referred to as magnetic shear, s, formally defined as

$$s = \frac{r}{q}\frac{\mathrm{d}q}{\mathrm{d}r} \ . \tag{6.8}$$

Magnetic shear plays an important role in the confinement and stability of tokamak plasmas.

The distribution of current inside a tokamak plasma, which is largely determined by the temperature profile via the plasma resistivity (see Sect. 6.2.4), influences the stability properties of the plasma, and its characterization is therefore an important aspect of plasma equilibrium analysis. It is common to characterize this distribution via the (normalized) internal inductance per unit length, l_i,

$$l_\mathrm{i} = \frac{< B_\theta^2 >_\mathrm{vol}}{< B_\theta^2(a) >_\mathrm{flux}} = \frac{4U_\mathrm{p}}{\mu_0 R_0 I_\mathrm{p}^2} \ , \tag{6.9}$$

where $< >_\mathrm{vol}$ represents a volume average and $< >_\mathrm{flux}$ a flux-surface average over the plasma boundary, $B_\theta(a)$ is the poloidal field at the plasma edge and U_p the poloidal field energy within the last closed flux surface. Typical values of l_i lie in the range 0.5-1.5.

Plasma pressure is not only the key parameter in fusion power production, but it also plays a crucial role in the stability properties of the plasma. Since a major consideration for a magnetic fusion reactor is the efficiency with which the magnetic field is used to confine the plasma pressure, it is usual to normalize the pressure to the magnetic field pressure,

$$\beta = \frac{\int p\,\mathrm{d}V}{V}\frac{2\mu_0}{B_\phi^2(0)} \ , \tag{6.10}$$

where p is the total pressure produced by all particle species within the plasma, V is the plasma volume, $B_\phi(0)$ is the toroidal magnetic field at the center of the plasma flux surfaces, and β is referred to as the *toroidal* beta. Certain aspects of equilibrium analysis also require the use of the *poloidal* beta,

$$\beta_\mathrm{p} = \frac{\int p\,\mathrm{d}V}{V}\frac{2\mu_0}{< B_\theta(a) >_\mathrm{line}^2} \ , \tag{6.11}$$

where $< >_\mathrm{line}$ represents an average around a poloidal line.

6.2.3 Particle orbits

Charged particles confined by a magnetic field follow helical paths composed of a gyration around the field lines, the Larmor orbit, and free motion along the field lines. The particle's motion can be visualized most simply as consisting of a Larmor orbit superimposed on the motion of a "guiding center" which follows the field lines. However, since the magnetic fields in a tokamak vary in magnitude and are curved as a result of toroidal geometry, particle trajectories deviate from the field lines in several ways. The simplest illustration of this effect is that the projection of the particle's guiding center trajectory in the poloidal plane does not lie precisely on the magnetic surface on which the particle is "confined", but is displaced slightly inwards or outwards by an amount,

$$\Delta r_{\mathrm{p}} \sim \varepsilon \rho_{\mathrm{L}\theta} = q \rho_{\mathrm{L}\phi} \ , \tag{6.12}$$

where $\rho_{\mathrm{L}\theta}$ is the Larmor radius in the poloidal field, and $\rho_{\mathrm{L}\phi}$ the Larmor radius in the toroidal field,

$$\rho_{\mathrm{L}} = \sqrt{2}\,\frac{m_j \upsilon_T}{\left|q_j\right| B} \ . \tag{6.13}$$

m_j and q_j are the electron (j = e) or ion (j = i) mass and charge respectively and υ_T the thermal velocity,

$$\upsilon_T = \sqrt{\frac{k_{\mathrm{B}} T_j}{m_j}} \ , \tag{6.14}$$

where T_j is the temperature.

Due to the gradient in toroidal field which particles experience as they travel from the large major radius to the small major radius side of the poloidal cross-section, "magnetic mirroring" can occur as a result of the conservation of the particle magnetic moment. This implies that a particle traveling through a region of increasing magnetic field strength must gradually transfer parallel momentum to perpendicular momentum. Thus, a particle with insufficient parallel velocity will be reflected by the magnetic mirror at the point in its guiding center trajectory at which the conservation of magnetic moment causes the parallel velocity to fall to zero. Such *trapped* particles are confined to the outer part of the poloidal cross-section and their resultant guiding center orbits, when projected into the poloidal plane, take the form of "bananas" with a half-width at the torus midplane,

$$\Delta r_{\mathrm{t}} \sim \varepsilon^{0.5} \rho_{\mathrm{L}\theta} \approx \frac{q \rho_{\mathrm{L}\phi}}{\varepsilon^{0.5}} \ . \tag{6.15}$$

In contrast, *passing* particles circle completely around a flux surface on orbits described by (6.12). Idealized banana orbits occur only in the absence of particle collisions and a significant fraction of trapped particles can exist only when the particle collision frequency is sufficiently low to allow particles to complete a banana orbit without experiencing a "detrapping" collision (see Sect. 6.4.1). Under such conditions, implying local plasma temperatures of at least several hundred eV to 1 keV, a fraction,

$$f = \left(\frac{2r}{R_0 + r} \right)^{0.5} \ , \tag{6.16}$$

of the particles at minor radius r is trapped. The existence of a population of trapped particles significantly influences the macroscopic properties of tokamak plasmas, as manifested in parameters such as the plasma resistivity and thermal diffusivity, and the description of plasma behavior in toroidal systems which includes such effects is known as "neoclassical" theory (e.g. [76H1, 79G1]).

6.2.4 Plasma resistivity

Plasma resistivity arises from collisions between electrons and ions. It determines the level of plasma current driven by the central solenoid flux swing in inductive operation, provides the initial source of plasma heating and plays a significant role in the behavior of a major class of plasma instabilities, known as "resistive" instabilities. The relationship between the inductive electric field, $\boldsymbol{E}$, the current density distribution, $\boldsymbol{j}$, and the resistivity, η, is defined by Ohm's law for a magnetized plasma,

$$\boldsymbol{E} + \boldsymbol{v} \times \boldsymbol{B} = \eta \boldsymbol{j} \,, \tag{6.17}$$

where $\boldsymbol{v}$ is the fluid velocity, $\boldsymbol{B}$ is the magnetic field, and the parameters in (6.17) are defined locally within the plasma. To obtain an expression for resistivity in terms of plasma parameters, two further quantities must be defined. The first is the effective charge,

$$Z_{\text{eff}} = \frac{\sum_i n_i Z_i^2}{\sum_i n_i Z_i} \,, \tag{6.18}$$

which expresses the average ionic charge number of a plasma which is a mixture of ions with atomic numbers, Z_i, and particle densities, n_i. Tokamak plasmas are principally composed of hydrogen isotopes, but small quantities of impurity ions (e.g. carbon, oxygen, iron etc.), typically at concentrations of a few percent or less, are produced by the interaction of plasma particles with the power handling surfaces and vacuum vessel walls. Helium is an additional, unavoidable, constituent of deuterium-tritium plasmas.

The second parameter is the Coulomb logarithm, which describes the average Coulomb interaction between electrons and ions which gives rise to the plasma resistivity:

$$\ln \Lambda_{\text{ei}} = 15.2 - \frac{1}{2} \ln(n_{\text{e}} / 10^{20}) + \ln(T_{\text{e}}) \quad (T_{\text{e}} \text{ in keV}) \,, \tag{6.19}$$

is the Coulomb logarithm, n_{e} is the electron particle density and T_{e} the plasma electron temperature. For plasma parameters of interest in modern tokamak experiments (and prospective D-T power plant designs) $\ln \Lambda_{\text{ei}}$ lies in the range 15…19.

The simplest form of the plasma resistivity parallel to the magnetic field, as originally evaluated by Spitzer and his co-workers [53S1], is

$$\begin{aligned} \eta_{\text{par}} &= 0.51 f(Z_{\text{eff}}) Z_{\text{eff}} \frac{m_{\text{e}}^{0.5} e^2 \ln \Lambda_{\text{ei}}}{3 \varepsilon_0^2 (2\pi k_{\text{B}} T_{\text{e}})^{1.5}} \\ &= 1.65 \times 10^{-9} f(Z_{\text{eff}}) Z_{\text{eff}} \frac{\ln \Lambda_{\text{ei}}}{T_{\text{e}}^{1.5}} \quad (\text{unit: } \Omega\text{m}, T_{\text{e}} \text{ in keV}) \,, \end{aligned} \tag{6.20}$$

where $f(Z_{\text{eff}})$ is a correction factor which is listed in Table 6.1 [53S1, 97W1].

Table 6.1. The factor $f(Z_{\text{eff}})$ of (6.20).

Z_{eff}	1	2	4	16	∞
$f(Z_{\text{eff}})$	1	0.85	0.74	0.63	0.58

In current tokamak experiments, with plasma temperatures in the range of 1 keV, the plasma resistivity is of the order of that of room temperature copper ($\approx 2 \times 10^{-8}$ Ωm), while at 10 keV the resistivity is more than an order of magnitude smaller. The efficiency of "ohmic" heating therefore decreases rapidly with increasing plasma temperature and, as discussed in Sect. 6.3.1, additional techniques must be applied to heat plasmas to the high temperatures required for thermonuclear power production.

An implicit assumption in this analysis is that the electron distribution function is Maxwellian. However, under some circumstances (e.g. following plasma disruptions – Sect. 6.5.3) a fraction of the electrons can be accelerated to high energies and form a "runaway electron" population. This can occur since the drag force on electrons varies as v_e^{-2}, where v_e is the electron velocity. In the presence of a high electric field, the high velocity electrons in the tail of the Maxwellian distribution can experience a net acceleration which increases with velocity and can reach energies of some 10 MeV (e.g. [89M1, 97W1]).

Neoclassical effects modify the relationship between the electric field and plasma current density in two ways. Firstly, trapped electrons cannot move freely around the torus, which causes an increase of the plasma resistivity. The strength of this effect depends on the local plasma aspect ratio, which determines the fraction of trapped particles (see (6.16)), and the extent to which collisions produce detrapping of electrons: significant neoclassical effects are generally observed for local plasma temperatures above ≈ 1 keV, when the frequency of collisions between trapped and passing electrons is sufficiently low. Full expressions for the "neoclassical resistivity" can be found in [81H1, 97W1], but an approximation which provides an estimate of the magnitude of the effect when detrapping is negligible is [77H1]:

$$\eta_{neo} \approx \frac{\eta_{par}}{(1-\varepsilon^{0.5})^2} \quad . \tag{6.21}$$

Experimental evidence for the existence of neoclassical resistivity has been obtained in JET [88C1], JT-60 [90K1] and the Tokamak Fusion Test Reactor (TFTR) in the United States [90Z1].

The second neoclassical effect is that an additional component of toroidal current is produced due to the exchange of momentum between passing and trapped particles. The magnitude of this additional current, known as the "bootstrap" current [71B1], depends on the density and temperature gradients, and, since it relies on the existence of trapped particles, is zero at the plasma axis. A detailed treatment may be found in [95K1, 97W1], but an estimate for its global contribution to the plasma current is given by:

$$I_{bs} \approx C\varepsilon^{0.5}\beta_p I_p \ , \tag{6.22}$$

where C is a profile dependent coefficient in the range 1/3…2/3. Studies on several tokamaks have established good agreement between the detailed theory of the bootstrap current and experimental measurements (e.g. [88Z1, 95K1]) and have demonstrated plasmas in which up to 80 % of the plasma current was driven by the bootstrap mechanism, as shown in Fig. 6.4. The detailed quantitative agreement obtained between theory and experiment in relation to neoclassical resistivity and the bootstrap current provides confidence in the accuracy of the neoclassical theory of toroidal plasma behavior.

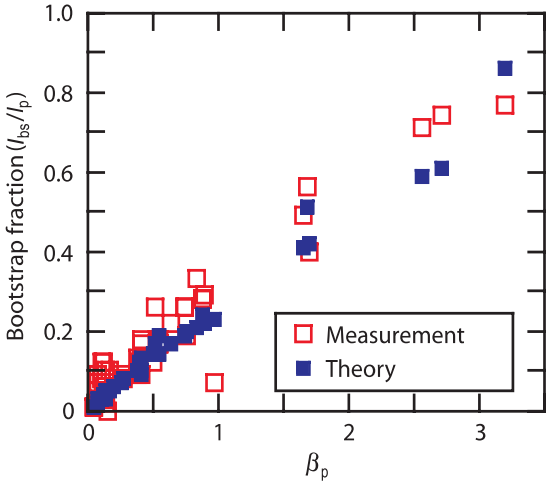

Fig. 6.4. Comparison of the experimentally derived and theoretically predicted bootstrap current fraction, I_{bs}/I_p, as a function of poloidal beta, β_p, in JT-60, illustrating the approximately linear relationship, see (6.22) [95K1].

6.3 Auxiliary systems

6.3.1 Heating and current drive systems

To attain the necessary plasma parameters for ignition, where α-particle heating can sustain the plasma temperature, the plasma must be heated in some way. Temperatures in the keV range can be produced by ohmic heating alone, but the efficiency of this process falls with increasing temperature and it is unlikely that tokamak plasmas can be heated to the required temperature by this means. Several auxiliary heating systems have therefore been developed to provide the required heating power, to allow non-inductive currents to be driven in the plasma, which is required if true steady-state operation is to be achieved (see Sect. 6.7), and to provide several sophisticated control capabilities (see Sect. 6.5.5).

Neutral beam injection (NBI) is based on the acceleration of positive hydrogen ions (including deuterium and tritium) to energies in the 100 keV range, their neutralization by a gas cell and the injection of the resultant intense beams of neutral particles across the plasma magnetic field. The energetic particles interact with thermal ions and electrons in the plasma, are ionized by several atomic processes, are then trapped in the confining magnetic field and gradually slow down, transferring their energy to the plasma ions and electrons, with a characteristic time for thermalization [72S1],

$$\tau_s = \frac{\tau_{se}}{3.0} \ln\left[1 + \left(\frac{E_b}{E_{crit}}\right)^{3/2}\right] , \tag{6.23}$$

where E_b is the beam energy, E_{crit} a critical energy defined below, τ_{se} is the characteristic slowing down time for ions on electrons,

$$\tau_{se} = \frac{3(2\pi)^{1.5}\varepsilon_0^2 m_p A_b (k_B T_e)^{1.5}}{\sqrt{m_e} n_e Z_b^2 e^4 \ln\Lambda_{ei}} , \tag{6.24}$$

Z_b and A_b are the atomic number and mass of the resultant fast ions. The critical energy is [94H1]

$$E_{crit} = 14.8 \; T_e \left(\frac{A_b^{3/2}}{n_e \ln\Lambda_{ei}} \sum_i \frac{n_i Z_i^2 \ln\Lambda_{ii}}{A_i}\right)^{2/3} \quad (T_e \text{ in keV}) , \tag{6.25}$$

where A_i and $\ln\Lambda_{ii}$ are the atomic mass and ion Coulomb logarithm (e.g. [97W1]) of thermal ions with density n_i. For energies above E_{crit}, the fast ions transfer their energy predominantly to electrons, while below the critical energy collisions with thermal ions constitute the main energy transfer mechanism. Systems capable of injecting up to 40 MW of 100 keV particles for periods of several seconds have been employed on the largest tokamaks to achieve the record ion temperature of ≈ 40 keV. Since the injected fast ion population represents an additional ion current, which produces drifts in the thermal electron and ion distributions as a result of Coulomb collisions, a non-inductive current is produced by NBI [70O1, 87F1]. The fast ion population also represents a source of external momentum, which can induce plasma toroidal rotation velocities orders of magnitude greater than in ohmic plasmas and which may influence transport processes within the plasma.

A significant change in technology is required for the next generation of tokamak experiments and for a power plant (see Sect. 6.10). In existing experiments, energetic neutral particles result from the neutralization of positive ions within the NBI system. However, to penetrate the larger and higher density plasmas characteristic of power plants, substantially higher particle energies, of order 1 MeV, are required. Since the charge exchange cross-section for positive ions falls rapidly with energy above ≈ 100 keV, it is necessary to develop NBI systems in which *negative* hydrogen ions are accelerated, for which the neutralization cross-section remains almost constant into the MeV range. The technological and physics issues associated with NBI are reviewed in [81H2], [91S1] and in Chap. 6 of [99I1].

The variety of electromagnetic wave modes which can propagate in a plasma and the associated resonant absorption processes which occur have encouraged the development of heating schemes which make use of radiofrequency waves in various regions of the electromagnetic spectrum (e.g. [91C1], [92S1] and Chap. 6 of [99I1]). A major advantage is that RF power sources can be located at some distance from the tokamak (up to 50 m) and the radiowaves can be transmitted over waveguide systems with high efficiency. Coupling of the RF waves to the plasma is perhaps the most challenging aspect of this approach, since in some methods the waves must pass through an evanescent layer at the plasma edge, and care must be taken to minimize the fraction of power reflected at the antenna-plasma interface. In addition, resonant reflection can occur inside the plasma and the heating scheme must be arranged to avoid the occurrence of reflecting layers between the antenna and the absorption layer.

Ion cyclotron radiofrequency heating (ICRF) exploits the propagation of the "fast magnetosonic wave" in the region of the ion cyclotron frequency and its harmonics, typically 30…120 MHz in present devices, and systems capable of producing up to 20 MW of power for many seconds are operational (e.g. [75S1, 96B1]). Heating of ions or electrons can occur when the general resonance condition,

$$\omega = n\omega_{cj} + k_{par} v_{par,j} \ , \tag{6.26}$$

is satisfied. Here ω is the wave frequency, k_{par} is the component of the wave vector parallel to the total magnetic field, $v_{par,j}$ is the component of the particle velocity parallel to the magnetic field, $n = 0, 1, 2\ldots$ is the cyclotron harmonic number, and ω_{cj} is the cyclotron frequency for ions (j = i) or electrons (j = e),

$$\omega_{cj} = \frac{|q_j| B}{m_j} \ . \tag{6.27}$$

The resonance condition, (6.26), permits localization of the heating profile in the vicinity of a preselected major radius by matching the wave frequency and magnetic field via (6.27). Wave refraction also plays a role, but in modern large experiments, heat deposition profiles with a half-width of ≈ 15 cm are obtained. The majority of ICRF experiments employ harmonic heating of a minority ion species (e.g. several percent of hydrogen in deuterium) to produce an energetic ion tail which transfers its energy predominantly to electrons – the physics of this process is again governed by (6.23) to (6.25). However, majority ion heating schemes and direct electron heating (with $n = 0$ in (6.26)) have also been used successfully. ICRF has, in addition, a current drive capability which has been observed in several experiments. When the parallel phase velocity of the RF wave matches the parallel velocity of an electron, the waves can impart net momentum to the electron. If the RF waves are phased so that momentum is transferred preferentially to electrons traveling either co or counter to the plasma current, a non-inductive current results. A similar interaction with minority plasma ions is possible, but the driven current has opposite phases on either side of the minority ion resonance location, allowing local modifications of the current profile.

Direct heating of electrons by wave absorption at the electron cyclotron frequency and its low harmonics (ECRF) is also used extensively (e.g. [83B1, 94E1]). This involves frequencies in the region of 30…140 GHz (increasing towards 200 GHz for power plant applications), where the "gyrotron" microwave power sources are a relatively new technology and remain under intensive development (e.g. [98T1]). As a result, ECRF systems are currently limited to power levels of several MW for 1…2 s. The general resonance condition for electron cyclotron absorption is as given by (6.26) and (6.27), but due to the higher thermal velocities of the electrons, the relativistic mass of the electron must be used in (6.27) and relativistic effects play an important role in the absorption process.

Coupling of ECRF waves to the plasma is less problematic than for other RF heating methods, since waves in this frequency range can cross the vacuum-plasma interface without attenuation or reflection. Reflecting layers can exist within the plasma, but the plasma parameters and heating frequency are generally arranged so that the waves propagate to the absorption layer without reflection. The cyclotron frequency increases linearly with the magnetic field, while the frequency at which reflection occurs increases as $n_e^{0.5}$, so the presence of unwanted reflecting layers is unlikely to be a problem in reactor-like plasmas. Further features of electron cyclotron absorption are that the wave is fully absorbed close to the resonance layer, the width of the resonance is narrow, so that power deposition profiles of only a few

centimeters can be achieved, and that current can be driven by preferentially coupling to the electrons traveling in one toroidal direction [87F1]. ECRF heating is therefore well suited to the control of plasma profiles and localized current drive can be used to control plasma instabilities (see Sect. 6.5.5).

The lower hybrid resonance is a coupled resonance of the ions and electrons,

$$\omega_{LH} = [(\omega_{ci}^2 + \omega_{pi}^2)^{-1} + (\omega_{ce}\omega_{ci})^{-1}]^{-0.5} , \tag{6.28}$$

where ω_{pi} is the ion plasma frequency,

$$\omega_{pi} = \left(\frac{n_i q_i^2}{m_i \varepsilon_0} \right)^{0.5} . \tag{6.29}$$

The electron plasma frequency, ω_{pe}, is defined analogously using n_e, q_e and m_e.

Though the associated heating and current drive technique is referred to as "lower hybrid wave heating" (LHW), the frequency range of interest lies above ω_{LH} and is typically in the region 1…8 GHz in present experiments (e.g. [99I1]). A key feature of lower hybrid waves is that they accelerate the small fraction of electrons whose velocity matches the phase velocity of the waves in the plasma to energies in the region of 100 keV via "electron Landau damping" (e.g. [87F1, 97W1]). If a toroidally asymmetric wave spectrum is launched, net momentum is imparted to the plasma electrons and an efficient current drive mechanism results. LHW systems in current experiments operate at the 10 MW level for many seconds and have allowed full non-inductive current drive to be achieved at plasma currents of 3 MA in JT-60U [95I1] and JET [95S1]. LHW is particularly attractive as a current drive technique, since in present devices its current drive efficiency, γ_{CD}, is greater than that of other auxiliary heating systems, where

$$\gamma_{CD} = \frac{n_e R_0 I_{CD}}{P_{aux}} , \tag{6.30}$$

with I_{CD} being the current driven by non-inductive means and P_{aux} the auxiliary heating power. Transmission of LHW through the plasma edge is problematic, however, as an evanescent layer appears if the plasma density in front of the "launcher" (i.e. antenna) falls too low. Since LHW does not involve resonant absorption, the power and current deposition in the plasma must be controlled by varying the spectrum of waves launched. As a result, the deposition profile is generally rather broad. Parasitic absorption processes involving energetic ions can also occur, and for next generation or reactor-like plasmas the LHW frequency must be at least 5 GHz to avoid absorption by α-particles.

Considerable progress has been made in developing the non-inductive current drive capability of auxiliary heating systems. To date, only LHCD has achieved current drive efficiencies close to those required for a power plant, $\gamma_{CD} > 0.3 \times 10^{20}$ AW^{-1}m^{-2} (e.g. [99I1]). Nevertheless, it is expected on theoretical grounds that the efficiency of most current drive schemes should increase linearly with electron temperature [87F1], a result which has been confirmed in several experiments (e.g. [99I1]). This implies that current drive efficiencies in power plants should increase by up to an order of magnitude for those current drive techniques (electron cyclotron, fast wave – in the ion cyclotron frequency range – and neutral beam) which are limited to rather low efficiencies, $\gamma_{CD} < 0.05 \times 10^{20}$ AW^{-1}m^{-2}, in present experiments due to the relatively low average electron temperature.

6.3.2 Fueling and exhaust

Plasma fueling systems must provide the initial gas for plasma breakdown, raise the plasma density to the required level and, in a power producing plasma, replace the deuterium and tritium fuel as it is consumed by thermonuclear reactions (e.g. [91P1] and Chap. 4 of [99I1]). In a reactor, the fueling requirements arising from the consumption of the deuterium-tritium fuel will be modest, amounting to only 7.1×10^{20} atoms/s of deuterium and tritium per gigawatt of fusion power (i.e. 1.35 Pam^{3}s^{-1} per GW), equivalent to ≈ 1 % of the total fuel content of the plasma. A far higher fueling demand will arise simply from the re-

quirement to maintain the plasma density high enough, i.e. $\approx 1 \times 10^{20}$ m^{-3}, for an acceptable reaction rate and from the need for efficient exhaust of helium "ash", as discussed below.

The majority of current tokamak experiments rely on gas-puffing for plasma fueling. There is no strong evidence to date that the number and distribution of gas inlet positions have a major influence on plasma behavior or fueling efficiency (the fraction of neutral gas which is ionized and contributes to the plasma density) (e.g. [01L1]). In present experiments, NBI can also contribute significantly to the plasma fueling and injects fuel deep within the plasma, but in reactor scale plasmas, the high beam injection energy required implies that NBI will make little contribution to fueling.

As plasma dimensions increase and higher plasma densities are achieved, the efficiency of the penetration of fuel from the edge to the core plasma is reduced and more effective fueling methods are required. The most highly developed alternative method involves the injection of small (a linear dimension of several mm) pellets of frozen hydrogen or deuterium, launched at velocities ranging from several hundred meters/s to several kilometers/s [95M1] and containing $\approx 1 \times 10^{21}$ atoms. In order to achieve high pellet repetition rates (10…100 Hz), centrifugal accelerators are employed. Although pellets can penetrate to the plasma center in some existing devices, the depth of pellet penetration into the plasma, λ_p, is found to scale as [97B1],

$$\lambda_p / a \propto T_e(0)^{-5/9} n_{e,20}^{-1/9} r_p^{5/9} v_p^{1/3} \ , \tag{6.31}$$

where $T_e(0)$ is the central electron temperature, $n_{e,20}$ is the electron density, r_p the equivalent spherical pellet radius and v_p is the pellet launch velocity, with units (keV, 10^{20}m^{-3}, m, ms^{-1}). Technological limitations will probably restrict repetitive pellet injectors to pellet launch velocities of $\approx 3 \times 10^3$ ms^{-1}, so it is unlikely that pellets will penetrate much beyond the outer 10…20 % of reactor scale plasmas. Nevertheless, this should substantially improve the fueling efficiency relative to gas fueling. The launching of pellets from the high field side of the plasma ("inside launch") is also found to enhance fueling efficiency, since transport processes within the plasma then sweep the material ablated from the pellet towards the plasma core [97L1]. One novel approach to plasma fueling, which is still at an early stage of development, but has been demonstrated on the Tokamak de Varennes in Canada [94R1], involves the injection of a small self-confined magnetoplasma known as a "compact toroid", which penetrates into the magnetic structure of the main plasma and deposits its own particles.

Pumping is an equally important aspect of plasma particle control, since the plasma density must be actively controlled, for example to control the fusion power production in a reactor. Moreover, the exhaust of helium "ash", i.e. α-particles which have slowed to the energy of the thermal plasma particles, is essential to avoid poisoning the plasma and terminating the burn: predictions for thermonuclear plasmas indicate that the helium concentration in the plasma must be kept below about 10 %. This condition can be characterized in terms of the plasma confinement properties by [90R1]

$$\tau_{He}^* / \tau_E < 15 \ , \tag{6.32}$$

where τ_{He}^* is the residence time for helium in the vacuum chamber,

$$\tau_{He}^* = \frac{\tau_{He}}{1 - \Re} \ , \tag{6.33}$$

τ_{He} is the global particle confinement time for helium and $\Re$ is the "recycling coefficient", i.e. the probability that a helium ion which escapes from the plasma will be reflected from the chamber wall or desorbed at some later time and re-enter the plasma. In experiments without helium pumping systems, recycling coefficients for helium are observed to be of order unity, so that τ_{He}^* can be orders of magnitude longer than the particle confinement time determined by plasma transport processes.

The pumping speed required for active particle control (typically ≈ 100 m^{3}s^{-1}) can be readily attained by cryopumps cooled to liquid helium temperatures. A helium pumping capability can be provided by coating the pumps with argon frost, but for reactor scale plasmas the use of activated charcoal is preferable (e.g. [98I1]). Both limiter and divertor tokamaks have operated successfully with cryopumps and have demonstrated efficient helium exhaust (see Sect. 6.6.3). Nevertheless, the requirements for helium

exhaust impose certain constraints on the fueling and exhaust requirements for a power plant. While the helium concentration in the core may be approximately 10 %, the helium concentration in the divertor plasma may be only a few percent (a process known as "enrichment", though in fact it corresponds to dilution). Since the pumping speeds for hydrogenic isotopes and for helium are very similar, this implies that ≈ 30 deuterium or tritium molecules are removed for every atom of helium. The helium production rate is 1.35 $Pa m^3 s^{-1}$ per GW, so that in steady-state operation helium must be exhausted from the vacuum chamber at this rate, implying that ≈ 40 $Pa m^3 s^{-1}$ of D-T fuel per GW must be pumped simultaneously. To maintain constant operating conditions, D-T fuel must therefore be supplied to the plasma at 30 times the rate implied by the level of fusion power production.

6.3.3 Diagnostics

Sophisticated measurement systems are incorporated into all modern tokamak experiments to allow the plasma parameters, such as density and temperature, to be determined (e.g. [87H1, 88O1, 98S1, 99I1]). These "plasma diagnostics", which monitor both the plasma and its interaction with the first wall, fulfill several functions: they provide information to real-time protection systems on the evolution of plasma parameters; they permit the plasma equilibrium and many other parameters to be controlled in real-time; they allow evaluation of the plasma performance (e.g. fusion power production) and analysis of the processes determining plasma behavior. The measurement techniques span virtually the entire electromagnetic spectrum, from DC to γ-rays, and include the analysis of various particle species (e.g. neutrons), as well as surface physics measurements of processes occurring at the plasma facing surfaces. Where possible, techniques have been developed which allow local measurements of plasma parameters with good spatial resolution (≈ $a/10$ is acceptable for many, though not all, applications), but in many cases the physical processes involved are such that "line integrated" measurements must be made along several (or many) chords through the plasma. In such cases local measurements may be obtained by making various forms of numerical data inversion (e.g. tomography) under certain assumptions about the symmetry of the plasma poloidal cross-section. Timescales also represent a significant issue for diagnostic systems: the plasma pulse may be tens of seconds long (and in power plants, thousands of seconds, or essentially steady-state), while a range of processes with timescales ranging from 100 μs upwards may influence the plasma behavior and perhaps require a real-time response.

The essential principles of many of these diagnostics remain unchanged at the power plant scale. However, the high radiation levels and heat fluxes, as well as the constraints on access through the shielding and tritium breeding blankets of a reactor, will require improvements in technology in several areas, most notably radiation resistance and resilience to heat and particle fluxes for components inside the vacuum chamber (e.g. elements of the magnetics, spectroscopic and plasma-wall interaction diagnostics). In addition, the long timescales will require precise corrections for drifts in electronic systems, for example in the integrators used in magnetic diagnostics for equilibrium shape control.

6.4 Transport and confinement

6.4.1 Elementary transport processes

The common measure of the quality of plasma confinement in a tokamak is the energy confinement time, τ_E, defined in (6.2), which is determined by local processes which transport energy from the plasma core to the edge: conduction, characterized by the thermal diffusivities for electrons, χ_e, and ions, χ_i; convection, characterized by the particle diffusion coefficient, D; and radiation. In toroidal confinement systems, magnetic field lines close within the torus and power is therefore lost by transport across field lines. The irreducible minimum transport rate is then set by Coulomb collisions between plasma particles. Toroidal geometry can significantly influence this minimum rate, firstly because the drifts associated with toroidal geometry (Sect. 6.1) are not completely canceled in the tokamak magnetic field, and secondly because the

average displacement of trapped particles from their confining flux surface is larger than that for passing particles (Eqs. (6.15) and (6.12) respectively), so that they can make larger radial steps as a result of collisions.

"Neoclassical" transport, the theoretical model which incorporates these effects is very highly developed (e.g. [76H1, 79G1, 89M1, 97W1]) and shows that the relative importance of the effects described above is determined by the plasma collisionality,

$$\nu_{*e} = (\varepsilon \tau_{ei} \omega_b)^{-1} \ , \tag{6.34}$$

where τ_{ei} is the electron-ion collision time and ω_b is the trapped particle "bounce" frequency,

$$\tau_{ei} = \frac{3(2\pi)^{1.5} \varepsilon_0^2 m_e^{0.5} (k_B T_e)^{1.5}}{n_i Z_i^2 e^4 \ln \Lambda_{ei}} \ , \tag{6.35}$$

$$\omega_b = \varepsilon^{0.5} \frac{v_T}{q R_0} \ . \tag{6.36}$$

Despite the quantitative success of neoclassical theory in predicting the correct level of plasma resistivity and bootstrap current (Sect. 6.2.4), measured transport losses are much worse than expected. Under some conditions, ion heat transport approaches the neoclassical value across some fraction of the plasma cross-section, though it is usually several times higher than predicted. Electron heat loss, however, is typically two orders of magnitude greater than the neoclassical value and is often the dominant heat loss channel. It is believed that the "anomalous" transport losses are due to small scale instabilities, or "turbulence", with wavelengths very much smaller than the plasma minor radius (e.g. [70B1, 94C1]). The proposed instabilities are driven by the free energy available in the plasma pressure and magnetic field profiles. They may be largely "electrostatic" in nature, in which case the electric fields cause enhanced particle drifts across the field lines, or "electromagnetic", causing the field lines themselves to be broken so that particles and energy can flow radially along field lines. While there is much experimental evidence for fine scale turbulence within tokamak plasmas and theoretical calculations indicate that a variety of suitable instabilities may exist, the experimental evidence relating specific instabilities to the enhanced transport found in toroidal plasmas is not yet conclusive.

In present tokamak experiments, heat loss due to radiation is dominated by line radiation from partially stripped impurity ions (i.e. ions retaining one or more bound electrons), though recombination radiation can make a contribution. However, the light impurities, such as carbon and oxygen, which are the main sources of plasma contamination, are fully ionized in the plasma core and radiate only near the plasma edge, in the region where the electron temperature is below a few hundred eV. This has the important consequence that the radiation may make a significant contribution to the global power balance, at the 20…50 % level, but has little impact on energy confinement. Radiation influences the energy confinement only when sufficient higher-Z impurities (e.g. iron, nickel etc.) are present, or there are excessive impurity influxes due to uncontrolled plasma-wall interactions. In reactor scale plasmas, two further sources of radiation can play a role in energy confinement [94S1, 97W1]: bremsstrahlung, which is emitted by electrons as they collide with ions, and electron cyclotron emission, radiated by electrons as they spiral in the confining magnetic field. Each could amount to 10…20 % of the α-particle power in a thermonuclear plasma. Taken together, therefore, they could reduce the energy confinement time by perhaps 20 %, and will play a significant, though not determining, role in plasma heat transport.

6.4.2 Plasma confinement modes

In the absence of a quantitative understanding of the processes determining plasma transport, a more empirical approach to the characterization of plasma confinement, referred to as "confinement scaling", has been developed. This relates the global energy confinement time to macroscopic plasma parameters and it has the merit that it offers a route to determining how large a device must be to achieve the energy confinement time required for ignition. Until recently, it was usual to measure the global energy confinement time, which includes the energy of energetic particle populations produced by auxiliary heating systems. However, since energetic particle populations can contribute significant fractions (≈ 20 %) of the total plasma energy under some conditions, and since the ignition condition depends on the energy confinement of the thermal plasma, the thermal energy confinement time is now preferred,

$$\tau_{E,\mathrm{th}} = \frac{\int \frac{3}{2}(n_\mathrm{e} k_\mathrm{B} T_\mathrm{e} + n_\mathrm{i} k_\mathrm{B} T_\mathrm{i})\,\mathrm{d}V}{P_\mathrm{OH} + P_\mathrm{aux} - \frac{\mathrm{d}W_\mathrm{th}}{\mathrm{d}t}} \ , \tag{6.37}$$

where P_OH is the ohmic input power, P_aux the auxiliary heating power and $\mathrm{d}W_\mathrm{th}/\mathrm{d}t$ corrects for the time rate of change of the thermal energy. In D-T plasmas, the denominator of (6.37) would also include the α-particle power, P_α.

The scaling behavior of the energy confinement time depends on plasma conditions, and several principal plasma confinement regimes, or "modes", have been identified. These correspond to tokamak operating conditions which are empirically reproducible, but for which there is incomplete understanding of the underlying physics. The simplest mode is the "ohmic heating" regime, where the plasma current provides the input power. At low plasma densities, the confinement scaling is referred to as "linear ohmic confinement" (LOC), since the energy confinement time increases linearly with the plasma density,

$$\tau_E^\mathrm{LOC} \approx 0.1 \ n_{\mathrm{e},20} R_0^2 a q^{0.5} \ (\mathrm{s}) \ , \tag{6.38}$$

where the dimensions for ($n_{\mathrm{e},20}$, R_0, a) are (10^{20} m^{-3}, m, m) [84G1]. Beyond a critical density, which varies from tokamak to tokamak, the energy confinement time remains constant as the density increases and the plasma is said to be in the "saturated ohmic confinement" regime (SOC). In cases where a peaked density profile can be sustained, for example by pellet injection, the LOC confinement behavior can be extended to higher densities.

As discussed in Sect. 6.3.1, auxiliary heating systems must be used to heat the plasma to thermonuclear conditions. In the early 1980s, experiments on several tokamaks showed that the plasma energy rose with auxiliary heating power, as expected, but that the energy confinement time invariably fell. The first systematic attempt to summarize this behavior is known as "Goldston" scaling [84G1],

$$\tau_E^\mathrm{G} = 0.037 I_\mathrm{p} P_\mathrm{loss}^{-0.5} \kappa^{0.5} R_0^{1.75} a^{-0.37} \ \ (\mathrm{s}) \ , \tag{6.39}$$

with (I_p, P_loss, R_0, a) having dimensions (MA, MW, m, m). This provides a good description of the global energy confinement in the standard mode of tokamak operation with auxiliary heating, which is referred to as the "L-mode" (or low confinement mode). In order to provide a more broadly based scaling expression for extrapolation to next generation tokamak experiments, such as ITER (see Sect. 6.10), a revised scaling for L-mode energy confinement has been derived from a more extensive confinement database which incorporates data from the most recent generation of tokamak experiments including JET, JT-60 and TFTR. This scaling is denoted ITER89-P [90Y1] (in reference to the year of its derivation),

$$\tau_E^\mathrm{ITER89-P} = 0.048 I_\mathrm{p}^{0.85} P_\mathrm{loss}^{-0.5} \kappa^{0.5} R_0^{1.2} a^{0.3} n_{\mathrm{e},20}^{0.1} B_0^{0.2} A^{0.5} \ (\mathrm{s}) \ , \tag{6.40}$$

where (I_p, P_loss, R_0, a, $n_{\mathrm{e},20}$, B_0) have dimensions (MA, MW, m, m, 10^{20} m^{-3}, T), B_0 is the toroidal field on the magnetic axis of the plasma and A is the average atomic mass of the plasma ions.

Several plasma regimes have been identified in which the global energy confinement exceeds that observed in L-mode plasmas by a factor of 2 or more (up to a factor of 4 in some experiments). The most reproducible of these is the high, or "H-mode", confinement regime, first observed in the ASDEX divertor tokamak in Germany as a bifurcation in the plasma state in which the energy confinement time suddenly increased by a factor of 2 [82W1]. Experiments in many tokamaks have confirmed the ASDEX observations and have documented the detailed phenomenology of the H-mode. It is most easily accessed in "diverted" plasmas, though in some cases H-mode plasmas have been obtained in limiter configurations (but more commonly with the limiter on the high field side of the plasma). Operationally, a certain level of input power is necessary to trigger a transition into the regime and it has been conjectured that this reflects a requirement on the (conducted and convected) power flux across the plasma separatrix. The characterization of this "threshold power" has shown that it depends on the magnetic field, plasma density, major radius and ion atomic mass, and an accepted form of the threshold power scaling for SNX diverted plasmas has been derived from data accumulated from several tokamaks [00S1],

$$P_{\mathrm{LH}} = 2.84 A^{-1} B_0^{0.82} n_{\mathrm{e},20}^{0.58} R_0^{1.0} a^{0.81} \quad (\mathrm{MW}) \ , \tag{6.41}$$

where the variables and units are as defined in (6.40).

The physics processes responsible for the H-mode transition are not fully understood, but the transition originates at the plasma edge, where the temperature and density profiles become very steep in a narrow layer, perhaps several centimetres wide, and from spectroscopic measurements it is seen that strong poloidal and toroidal plasma flows can occur in this region. The steep pressure profiles and plasma flows require the existence of a radial electric field, E_r, to ensure force balance in the plasma, as illustrated by the lowest order radial force balance equation for a single ion species,

$$E_\mathrm{r} = \frac{1}{Z_\mathrm{i} e n_\mathrm{i}} \frac{\mathrm{d}p_\mathrm{i}}{\mathrm{d}r} - \upsilon_\theta B_\phi + \upsilon_\phi B_\theta \ , \tag{6.42}$$

where the species has an ionic charge Z_i, density n_i, pressure p_i, and poloidal and toroidal rotation velocities υ_θ and υ_ϕ respectively. Equation (6.42) provides the basis for a widely accepted explanation of the H-mode transition: a gradient develops in the radial electric field in the narrow edge region (for reasons which are not fully understood) which produces sheared plasma flows due to the $\boldsymbol{E} \times \boldsymbol{B}$ drift. This "flow shear" suppresses the growth of electrostatic instabilities thought to be responsible for the anomalous transport in L-mode plasmas (e.g. [94B1]). Microwave scattering measurements of the level of density fluctuations in this "edge transport barrier", or "pedestal", confirm that the fluctuation amplitude falls rapidly (within 100 μs) at the H-mode transition.

The evolution of the edge pedestal also controls the quasi-steady-state behavior of the H-mode via a repetitive plasma instability known as an "edge localized mode", or ELM (see Sect. 6.5.5). Following the H-mode transition, the edge pressure rises until a stability limit is reached and an ELM occurs, causing the pedestal density and temperature to fall. The instability then decays, allowing the pedestal pressure to rise again towards the stability limit. This repetitive behavior, occurring with a frequency in the range 10…1000 Hz (which depends on many parameters, but generally decreases with increasing plasma size), maintains the plasma in an approximate steady-state: "ELMy" H-modes have been sustained for up to 20 s, limited only by the pulse length of tokamak heating systems, a steady-state capability which makes the ELMy H-mode an attractive regime for power producing plasmas.

As for the L-mode, several scaling expressions have been developed to describe the dependence of H-mode energy confinement on plasma parameters. This work is still evolving, but the most recent expression for the thermal energy confinement time, known as the IPB98(y,2) scaling (ITER Physics Basis 1998 ELMy H-mode scaling #2), is [99I1]:

$$\tau_{E,\mathrm{th}}^{\mathrm{IPB98(y,2)}} = 0.144 I_\mathrm{p}^{0.93} P_\mathrm{loss}^{-0.69} \kappa_\mathrm{eff}^{0.78} \varepsilon^{0.58} R_0^{1.97} n_{\mathrm{e},20}^{0.41} B_0^{0.15} A^{0.19} \quad (\mathrm{s}) \ , \tag{6.43}$$

where the variables and units are as in (6.40), except that $\kappa_\mathrm{eff} = S/\pi a^2$ and S is the area of the plasma poloidal cross-section. The range of data from which this scaling has been derived and the extrapolation to a power producing tokamak such as ITER is illustrated in Fig. 6.5.

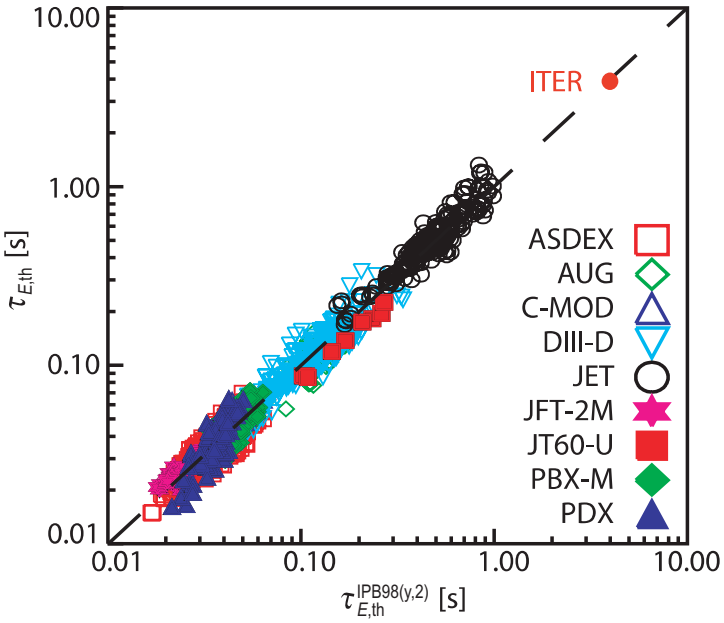

Fig. 6.5. Comparison of experimental values of thermal energy confinement times, $\tau_{E,th}$, and the fitted values according to the IPB98(y,2) confinement scaling for ELMy H-mode plasmas, (6.43). The tokamaks from which the data was obtained are indicated and the point labeled "ITER" is the extrapolation of energy confinement time to the proposed thermonuclear power producing tokamak of this name [02I1] discussed in Sect. 6.10.1.

Several additional plasma regimes with confinement characteristics of the H-mode have been observed, of which the earliest was the ELM-free H-mode. In these plasmas ELMs are suppressed for periods of several seconds. However, the plasma density, impurity content and impurity radiation often rise throughout the ELM-free phase and this eventually causes a return to L-mode. The energy confinement can rise above conventional H-mode levels, but the regime is invariably transient. Carefully prepared discharges in JET and DIII-D, a US experiment, have transiently achieved confinement enhancement factors of 3…4 relative to L-mode values. In DIII-D the regime is referred to as the "VH-mode" [91J1], while in JET a similar regime is referred to as the "hot-ion H-mode" (e.g. [92J1]), since the central ion temperature reaches 20…30 keV and may be a factor of 2 or more higher than the central electron temperature due to the injection of high power neutral beams into a low density target plasma. Quasi-steady-state H-modes with radiated power essentially equal to the input power have been produced by the deliberate introduction of additional impurities (usually noble gases such as neon). The regime, denoted "CDH-mode" (Completely Detached H-mode), was initially demonstrated in the ASDEX Upgrade tokamak [95G1] and may have important benefits for the reduction of heat fluxes onto power handling surfaces in a reactor. A related regime in a limiter configuration has been developed in the TEXTOR experiment, also located in Germany: the "RI-mode" (Radiation Improved mode) [96M1], again exploits the "seeding" of noble gases to increase the radiated power fraction. It is found that the energy confinement improves spontaneously and an essentially steady-state regime develops with energy confinement equivalent to that of an H-mode. A further important regime of improved confinement in limiter plasmas, the "supershot" [87S1] developed in TFTR, is discussed in Sect. 6.9.2.

Improvements in energy confinement are also observed in plasmas in which the magnetic shear close to the plasma center approaches zero or is reversed. In such "negative central shear" (NCS) or "optimized shear" (OS) plasmas, the transport losses are substantially reduced and the stability properties are improved. In the low shear region both heat transport through the ions and particle transport can fall to values commensurate with those predicted by neoclassical theory and in some cases the electron heat loss is also reduced. The development of a region of reduced transport in such plasmas is understood in terms of the formation of an "internal transport barrier" (ITB), by analogy with the edge transport barrier of the H-mode. Its occurrence allows the development of a steep pressure gradient in the plasma core, as illustrated in Fig. 6.6, which enhances the bootstrap contribution to the plasma current and has significant implications for steady-state operation of tokamaks (see Sect. 6.7). The first evidence for this phenomenon was obtained in JET in experiments in which the injection of deuterium pellets was used to arrest the development of the central current profile [91T1] and this was followed by significant advances in TFTR [95L1] and DIII-D [95S2].

Internal transport barriers may be produced in plasmas with either an L- or H-mode edge and with global energy confinement which is typically a factor of 2…3 greater than that of equivalent L-mode plasmas (with L-mode confinement defined by (6.40)). However, the predominantly transient nature of the regime and the range of phenomena observed, in terms of central shear, reduction in transport, relative effect on ion and electron transport, stability properties and radial width of the ITB region, have to date prevented the development of a coherent description of the regime, even at the simplest level of an energy confinement scaling. Experiments have demonstrated that some additional factor, other than reversed shear in the plasma core, is required to produce an ITB. The most favored explanation is that, as in the H-mode edge transport barrier, $\boldsymbol{E} \times \boldsymbol{B}$ driven velocity shear within plasma flows suppresses the turbulence which determines the level of L- or H-mode core transport. In some cases, it is thought that the development of a steep pressure gradient may itself make a contribution to the gradient in the radial component of the electric field (see (6.42)).

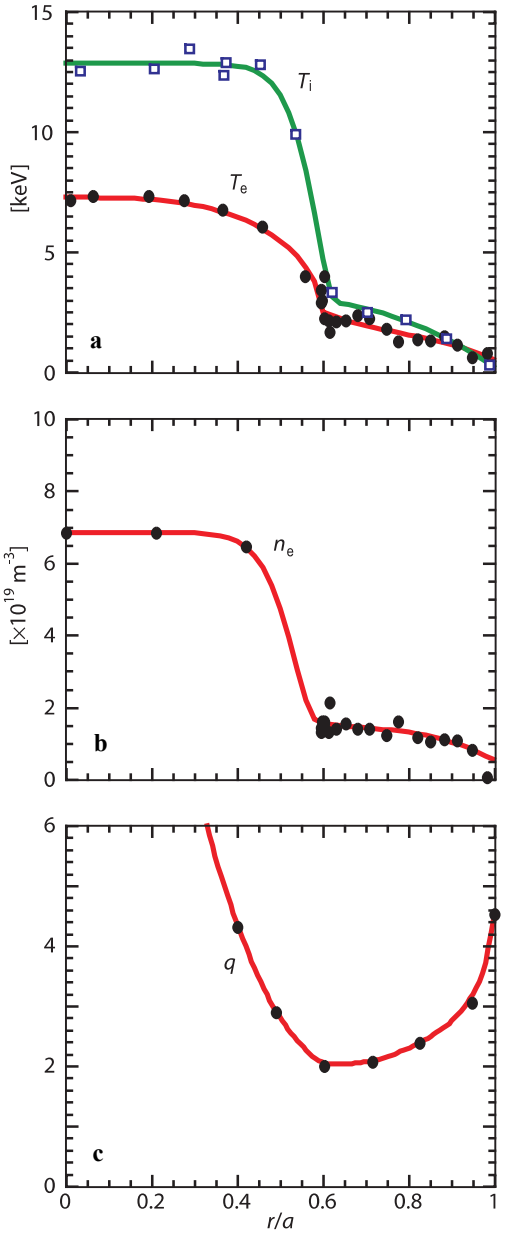

Fig. 6.6. Radial profiles from a plasma in JT-60U with an "internal transport barrier" (ITB): **(a)** ion and electron temperature, T_i and T_e respectively; **(b)** electron density, n_e; **(c)** safety factor, q. The steep gradients characteristic of the ITB, in (a) and (b), and the region of negative central shear, in (c), are readily identified [00O1].

6.5 Magnetohydrodynamic (mhd) stability

6.5.1 Essential principles

Magnetohydrodynamic (mhd) theory describes the stability properties of a plasma fluid immersed in a magnetic field. It encompasses both *global* stability, i.e. whether a plasma configuration of the type discussed in Sect. 6.2 can be maintained using external coils (e.g. [66S1]), and *local* stability, which involves an analysis of the balance between destabilizing and stabilizing effects at each magnetic surface [78B1, 87F2, 97W1]. Its significance for fusion performance is that the accessible operating space, in terms of plasma current, plasma pressure and plasma density, is defined by mhd stability considerations. The theory of mhd stability of toroidal plasmas is highly developed and provides an excellent qualitative, and in many cases quantitative, description of plasma behavior.

Two general classes of mhd instabilities can be identified. *Ideal* instabilities would occur even if the plasma were perfectly conducting and they involve motions in which the plasma and magnetic field are essentially "frozen" together. *Resistive* instabilities involve the small but finite plasma resistivity (Sect. 6.2.4) and produce rearrangements of the magnetic field topology by tearing and reconnection of the field lines, giving rise to the alternative terminology of "tearing modes". Both forms of instability have an infinite spectrum of possible modes. In tokamak plasmas these are described by poloidal and toroidal mode numbers (m, n) which characterize the number of nodes in the poloidal and toroidal directions respectively. Unstable modes grow initially in the vicinity of the magnetic surface having $q = m/n$, for which the magnetic field helix corresponds to that of the mode, but modes with low values of m and n can develop significant perturbations over a substantial fraction of the plasma minor radius. The safety factor profile therefore plays a key role in the determination of global and local plasma stability.

In the case of resistive instabilities, the non-linear phase arising from the tearing and reconnection of field lines involves the formation of a "magnetic island" having a different magnetic topology from the remainder of the plasma. Nested magnetic surfaces exist within the island which can "short-circuit" heat and particle fluxes radially across the island width, resulting in a degradation of the plasma confinement properties. However, the most important consequence of the growth of ideal and resistive modes is that the perturbation associated with one or more modes can grow to large amplitude across the entire plasma cross-section, leading to a "major disruption", which involves the loss of the plasma thermal energy and current on timescales of 1…10 ms in present experiments (Sect. 6.5.3).

6.5.2 Vertical instability

Elongated equilibria are favored for most current experiments and future fusion reactors, since, for a given value of edge safety factor, they allow a higher plasma current (see (6.7)) and hence higher energy confinement time (see (6.43)). Nevertheless, elongated plasmas are unstable against vertical displacements and the plasma equilibrium must be maintained by active feedback control via the PF coils (e.g. [93G1, 97W1]). When the feedback control system fails, or plasma parameters change too rapidly for the control system to respond (as in a major disruption – see Sect. 6.5.3), a vertical instability or "vertical displacement event" (VDE) can develop. This mode is toroidally symmetric and hence has toroidal mode number $n = 0$. In the absence of any toroidal conducting structure, an elongated plasma would be unstable on an "inertial" or "mhd" timescale,

$$\tau_{\mathrm{mhd}} = \frac{a}{V_{\mathrm{A}}} = \frac{a(\mu_0 \rho_m)^{0.5}}{B} \quad , \tag{6.44}$$

where V_{A} is the Alfvén velocity and ρ_m the plasma mass density. In current tokamak experiments $\tau_{\mathrm{mhd}} \approx 10^{-7}$ s and the plasma would be uncontrollable were it not for the stabilizing force which arises from currents induced in the vessel by the plasma motion. As a result of this interaction, the timescale for the growth of a vertical instability is of the order of the resistive penetration time of the vessel (together with any associated conducting structures), which is in the range 1…100 ms in many current experiments

and may be close to 1 s in fusion reactors. This permits fast feedback control systems to apply correction fields via the PF coils to stabilize the plasma vertical motion and has allowed plasmas with $\kappa \approx 2.5$ to be established in tokamaks such as DIII-D [90L1] and the Swiss tokamak TCV [98H1].

Vertical instabilities cause substantial forces on the vacuum vessel and in-vessel structures due to eddy currents induced in the vessel by the plasma motion and "halo" currents flowing between the plasma and the vessel via plasma facing components (PFC). Halo currents are induced by the change in toroidal flux which occurs during the vertical motion. They follow the helical field lines around the plasma edge and then follow an essentially poloidal path inside the vacuum vessel. In extreme cases, the resultant electromagnetic force on the vacuum vessel can amount to $\approx 10^7$ MN in existing experiments and up to $\approx 10^8$ MN in reactor scale devices. The plasma may become helically distorted as it moves vertically, causing a toroidally asymmetric distribution of halo currents and forces which can result in a significant radial force on the vessel. The mechanical design of fusion reactors will need to reflect such constraints as well as the very high thermal loads, up to 100 MJ m^{-2}, to which sections of the PFCs can be subjected.

6.5.3 Disruptions

Exceeding current, pressure and density limits in tokamak plasmas can give rise to mhd instabilities which grow to large amplitude and generate a major disruption. In these events the plasma thermal energy is typically lost in a few milliseconds and the plasma current (and hence poloidal field energy) is quenched in 1…10 ms. The sequence of events leading to a major disruption is well documented (e.g. [89W1, 95S3]) and it has been determined that disruptions are most often initiated by a resistive mhd mode – though in some cases ideal mhd instabilities are responsible – which is triggered by exceeding a local stability criterion. The initial phase of a disruption may last from several milliseconds to several hundred milliseconds, during which mhd modes grow and "minor disruptions" can occur (these disturb, but do not terminate, the plasma). Eventually, a rapid growth of one or more mhd modes occurs, affecting most of the plasma cross-section and leading to a rapid loss of the plasma thermal energy, which occurs in two phases lasting up to several milliseconds overall (see Fig. 6.7, illustrating the final phase of a major disruption in JET): the plasma cools rapidly to temperatures of a few eV due to both rapid transport along reconnected field lines and a massive increase in radiation following an influx of impurities from the first wall of the plasma chamber; plasma resistivity (see (6.20)) increases by several orders of magnitude due to the cooling and impurity influx; and the plasma current decays with the characteristic inductive decay time of the cold, impure plasma, i.e. several milliseconds.

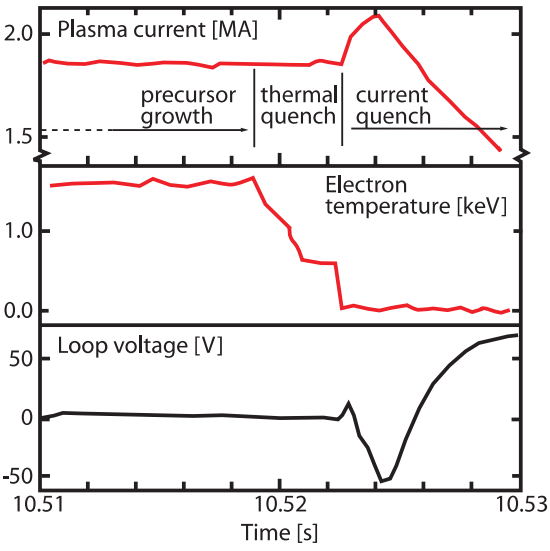

Fig. 6.7. The terminating events involved in a major disruption in JET showing the two phases of the thermal energy quench, characterized here by the electron temperature, which exhibits a "slow" decay around 10.52 s, and a "fast" decay at 10.522 s. This is followed by a short-lived 10 % positive spike in the plasma current, associated with the characteristic negative spike in the plasma loop voltage, and thereafter by the rapid decay of the plasma current [89W1].

In reactor scale plasmas, timescales for the energy and current quenches are expected to be an order of magnitude longer than in existing tokamaks (e.g. [99I1]), but the consequences of disruptions will nevertheless be severe and will impose significant design constraints on tokamak power plants. The principal concerns arising from disruptions in reactor plasmas include high heat loads, up to 100 $MJ\,m^{-2}$, on the first wall and divertor targets due to the rapid loss of thermal energy. In addition, substantial electromechanical forces ($\approx 10^8$ MN) would be produced in the vessel structures by eddy currents associated with the rapid current quench and related changes in the toroidal flux, as well as by halo currents produced by the VDE which often occurs during the current decay phase. Finally, large runaway electron currents can be generated in the cold post-disruptive plasma, with runaway currents amounting to perhaps 50 % of the initial plasma current [97R1]. With typical energies of 10…15 MeV, such runaway electron populations could produce damage on first wall structures when they are lost from the plasma.

Significant advances have been made in the development of techniques for the avoidance and mitigation of disruptions (e.g. [99I1]). There is now considerable quantitative understanding of disruption boundaries (e.g. see Sect. 6.5.4), which allows the trajectory of the plasma parameters to be controlled so as to avoid many of the conditions which could initiate disruptions. Techniques have also been developed to mitigate the most severe effects of disruptions, for example by the use of "killer pellets". Consisting of moderate-Z impurities such as neon or argon, or of deuterium doped with low levels of high-Z impurity such as krypton, these cryogenic pellets are ablated within the plasma, leading to massive impurity radiation which dissipates most of the plasma thermal energy and leads to a rapid (≈ 10 ms) quenching of the plasma current.

6.5.4 Operational limits

Three principal global stability limits have been identified, relating to the maximum plasma current, plasma pressure and plasma density which can be maintained. The limit relating to plasma current is due to the link between plasma current and the edge safety factor, $q(a)$ or q_{95} (see (6.7)). Experiments have demonstrated that as the plasma current increases and the edge safety factor falls to 2 (approximated by q_{95} in magnetic separatrix plasmas), an $m = 2$, $n = 1$ mode grows rapidly, producing a major disruption on timescales as short as a few milliseconds (e.g. [89W1]). Although stable and reliable plasma operation can be maintained in quasi-steady-state conditions in the region $2 \le q(a) \le 3$, plasmas with $q(a)$ in this range can be more sensitive to several of the instabilities discussed in Sect. 6.5.5. Therefore, although (6.40) and (6.43) indicate that it is advantageous to operate tokamak plasmas at the highest possible current for a given set of configurational parameters (a, R_0, B_0,…), it is usual to operate with $q(a)$ (or q_{95}) ≈ 3, to allow some margin against mhd instability.

At temperatures around 10 keV, the cross-section for the D-T reaction varies approximately as T^2. From (6.10), fusion power production therefore scales as $\beta^2 B_\phi^4$ and there is a considerable incentive to operate at the highest attainable β to make efficient use of the confining magnetic field. If tokamak power plants are to be economically viable, β must reach values of several percent or greater (e.g. [94S1]). In the DIII-D tokamak, β values of up to 12.5 % have been achieved for periods much shorter than 1 s and values of 8 % have been maintained for ≈ 1 s (e.g. [94S2]), while the "spherical tokamak" START in the United Kingdom (Sect. 6.9) has reached values as high as 40 % for about 1 ms [97S1].

The β value which can be attained and the nature of the limiting mhd instability depend on the plasma current and pressure profiles. From a stability analysis of ideal modes in plasmas with optimized (in terms of mhd stability) current and pressure profiles, a general scaling of the ideal β-limit has been derived [81S1, 84T1], which takes the form

$$\beta_{\mathrm{N,max}} = \beta_{\max}(\%)\frac{a(\mathrm{m})B_\phi(\mathrm{T})}{I_\mathrm{p}(\mathrm{MA})} \approx 3.5 \ . \tag{6.45}$$

The "normalized beta", β_N, is taken as a figure of merit for the β which is obtained in a given experiment. While the numerical value of $\beta_{\mathrm{N,max}}$ given in (6.45) has been found to approximate the upper bound to β

achieved experimentally, a correction to the β-limit scaling has been proposed on the basis of experimental data to reflect the dependence on current profile which is also observed (e.g. [94S2]),

$$\beta_{N,max} \approx 4 l_i \ . \tag{6.46}$$

Figure 6.8 shows a selection of data from a range of tokamaks for which β is plotted against I_p/aB_ϕ, illustrating that (6.45) provides a good description of much of the database. Some points clearly exceed the theoretical boundary and these are ascribed either to current profile effects (e.g. [92L1]), or to an effect referred to as "wall stabilization", in which the proximity of the conducting wall of the vacuum vessel transiently stabilizes a rotating ideal mode which would otherwise be unstable (e.g. [94B2]).

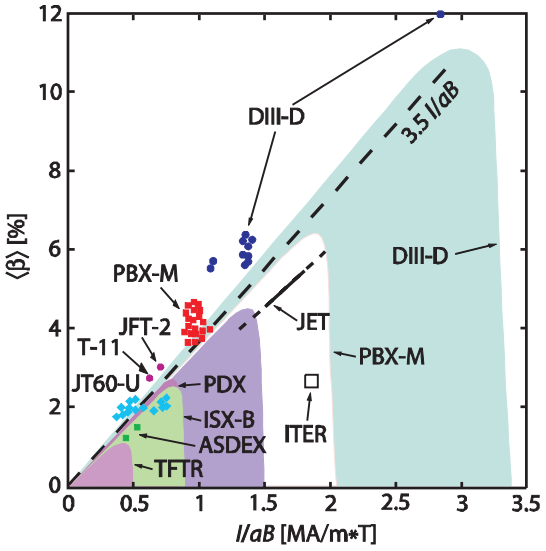

Fig. 6.8. A selection of data from a range of tokamaks showing the value of volume averaged β versus the normalizing factor I/aB and indicating that much of the data is bounded by the line $<\beta> = 3.5 I/aB$ [99I1].

The plasma density at which reactor plasmas are expected to operate, $> 10^{20}$ m^{-3}, is determined by several constraints, including the need to make effective use of the plasma β, since lower densities imply average temperatures well above 10 keV, at which the D-T reaction cross-section no longer scales as strongly as T^2. In addition, it is essential to reduce the power flux to plasma facing surfaces to acceptable values (roughly 10 MW m^{-2}) and to minimize impurity production at these surfaces, implying operation at low edge temperature and high edge density. High density is also favored by the H-mode energy confinement time scaling (see (6.43)), which shows the confinement time increasing with $n_e^{0.41}$.

The plasma density is limited by several phenomena linked to mhd stability. The ultimate limit, generally observed in L-mode plasmas, is set by radiation and/or transport instabilities in the plasma edge and scrape-off layer (SOL). These cool the plasma edge, triggering the growth of mhd instabilities and leading to a major disruption (e.g. [89W1]). This limit depends on the balance between input power and losses due to radiation and transport and so increases with input power (e.g. [99I1]). It is determined by the edge density, since impurity line radiation is emitted predominantly from the plasma edge and its intensity varies approximately as $n_{e,edge} n_{Z,edge}$, where $n_{Z,edge}$ is the density of the principal impurity just inside the LCFS. The average plasma density can therefore be extended beyond the limit observed in gas fueled discharges by pellet injection (Sect. 6.3.2), which deposits the fuel in the plasma interior. A second limiting process is observed in H-mode plasmas and may therefore be of more direct relevance to power production in reactors: it has been established in numerous experiments that it is difficult to maintain H-mode confinement while increasing the density above the "Greenwald" value [88G1],

$$n_{GW}(10^{20}\,\mathrm{m}^{-3}) = \frac{I_p(\mathrm{MA})}{\pi a^2(\mathrm{m})} \ . \tag{6.47}$$

This limit is manifested as a gradual degradation of H-mode energy confinement which eventually results in a return to L-mode. For a fusion power plant, this limit is of the same order as the minimum density set by the constraints outlined above and it therefore represents a critical issue for the development of power producing plasmas. The observation in JET [99S1] and other experiments, that the density at which confinement degradation occurs increases as the plasma triangularity increases (leading to increased edge magnetic shear and improving the edge mhd stability limit), is therefore of considerable importance. As noted in Sect. 6.3.2, inside launch pellet injection has also been exploited to increase the plasma density somewhat beyond the Greenwald value while maintaining H-mode quality confinement [97L1].

6.5.5 Mhd instabilities

In tokamaks, several repetitive instabilities can occur, leading to some tolerable degradation of confinement which is generally considered acceptable in exchange for the instabilities' role in maintaining quasi-steady-state conditions within the plasma. The most common instability is the "sawtooth" [74V1] which manifests itself as a periodic relaxation of the central plasma density and temperatures with a frequency which varies from ≈ 1 kHz during the ohmic heating phase of small tokamaks to less than 1 Hz during high power auxiliary heating in the largest devices (Fig. 6.9). Sawteeth are produced by an $m = 1$, $n = 1$ instability in the vicinity of the $q = 1$ surface in the plasma core, and the repetitive nature of the instability is due to the balance established between inward (resistive) diffusion of the plasma current and the redistribution of current produced by the sawtooth. The central temperature modulation shown is inverted beyond a certain minor radius (the "inversion radius", r_i), so that following the sawtooth "crash" the density and temperature profiles are flattened across the central region of the plasma, out to perhaps 50 % of the minor radius, but there is no direct loss of particles or energy from the plasma.

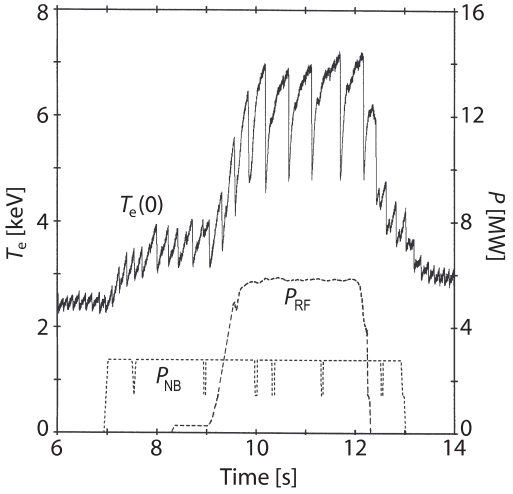

Fig. 6.9. Modulation of central electron temperature, $T_e(0)$, during sawtooth activity in ohmic and additionally heated phases of a plasma in the JET tokamak. P_{NB} indicates the waveform of the neutral beam injection heating and P_{RF} that of the ion cyclotron resonance heating.

Edge localized modes play an important role in controlling the plasma behavior in H-modes by causing a relaxation of the density and temperature gradients in the vicinity of the narrow edge pedestal (see Sect. 6.4.2). The rapid, ≈ 100 μs, loss of particles and energy from the plasma produces increased recycling on the divertor targets and PFCs which generates the signature ELM spike in the H_α spectroscopic signal. ELMs are classified into 3 broad categories, Type I ("giant"), Type II ("grassy"), or Type III ("transition"), according to their detailed characteristics and the region of parameter space in which they are observed (e.g. [96Z1, 98C1]).

Neoclassical tearing modes (NTM) [95C1, 97S2] grow as a result of an instability in the bootstrap current (Sect. 6.2.4) within a magnetic island. In collisionless plasmas, the flattened pressure profile within a magnetic island reduces the bootstrap current inside the island, increasing the deficit of current relative to the adjacent plasma and causing the island width to increase. In order for the bootstrap current

instability to influence the growth of the island, a certain minimum island size, or "seed" island, is required. This is commonly generated by other forms of mhd, such as sawteeth or ELMs, which can couple to resonant q-surfaces within the plasma. NTMs with $m = 3$, $n = 2$, or $m = 2$, $n = 1$ have become the most common mechanism for limiting β_N in ELMy H-mode plasmas, the limit typically occurring in the range 50…100 % of the ideal β-limit. However, the long timescale for the growth of the modes, several hundred milliseconds in present experiments, several tens of seconds at the reactor scale, allows feedback control of the modes, for example by driving current within the island to counteract the bootstrap current deficit (e.g. [99G1, 00G1]), as demonstrated in ASDEX Upgrade and other devices.

Resistive wall modes (RWM) (e.g. [94B2]) could become a significant limitation for high-β operation in regimes relevant to non-inductive steady-state operation of a tokamak. The RWM is a slowly rotating ideal mode with a frequency which is of the order of the inverse wall penetration time of the vacuum vessel ($\omega_{RWM}\tau_{wall} \approx 1$). Limitation of β by a disruption triggered by an $m = 3$, $n = 1$ RWM has been observed in DIII-D [95S4, 99G2]. RWMs are potentially amenable to stabilization by means of external feedback coils (e.g. [96F1]), and such schemes are under development [99G2].

6.6 Plasma-surface interactions

6.6.1 Power and particle control

The control of power and particle flows in a fusion power plant has a central bearing on both the performance of the burning plasma and on the integrity of the plasma facing components. Several hundred megawatts of power deposited in the plasma by α-particles must be exhausted without exceeding the power handling capability of the first wall, limited to ≈ 10…15 MW m^{-2} by engineering constraints, while avoiding excessive impurity production, which would contaminate the plasma and quench the thermonuclear burn. Impurity production is also inextricably linked to erosion of first wall materials, and erosion rates must be limited to ensure an adequate lifetime for surfaces in contact with the plasma edge – rapid erosion would imply frequent replacement of first wall materials, making operation of a fusion power plant uneconomic. Selection of the optimum plasma facing materials therefore involves a compromise among several considerations in addition to the obvious need to sustain high heat fluxes. A further requirement is that thermalized α-particles, or "helium ash", must be pumped away from the plasma edge to avoid poisoning the plasma and slowing the reaction rate.

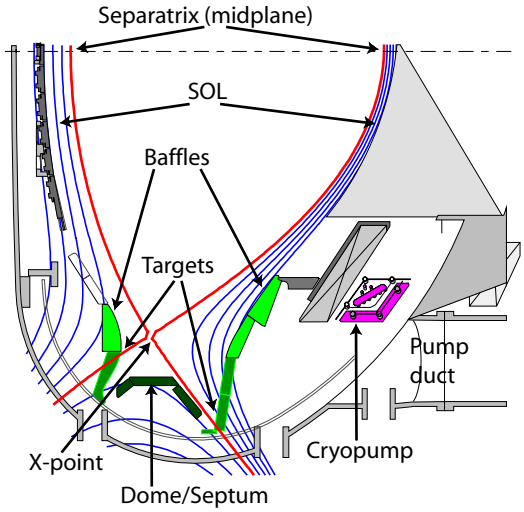

Fig. 6.10. Poloidal cross-section of the divertor region in the ASDEX Upgrade tokamak (see Fig. 6.3), illustrating the main elements of the divertor configuration. The regions where magnetic field lines intersect the divertor target plates are referred to as the "strike regions" and the intersection of the separatrix with the targets as the "strike points".

In present experiments, where power handling requirements are less demanding, since there is little thermonuclear power, two fundamental approaches to controlling the interaction between the plasma and the first wall have been developed, the "limiter" and "divertor" configurations, which were introduced in Sect. 6.2.1. The weight of current experimental experience suggests that a "poloidal divertor" configuration, as illustrated in Fig. 6.10, will have certain advantages in the reactor context in relation to both core plasma performance and the control of plasma-surface interactions, though this question remains the focus of extensive debate. The following discussion therefore concentrates on this configuration, but many of the basic physics processes are common to both concepts. Detailed treatments of the issues discussed here can be found in [90S1, 97P1, 97W1, 00S2] and in Chap. 4 of [99I1].

6.6.2 Plasma boundary issues

Outside the last closed flux surface, plasma continues to diffuse across the magnetic field lines. However, transport along the field lines is much more rapid and, since the open field lines in the scrape-off layer eventually intersect material surfaces (i.e. the PFCs), power and particles are preferentially lost along the field lines. Plasma radial profiles in the SOL take an exponential form with characteristic fall-off lengths, denoted λ_n, λ_T, and λ_P respectively for density, temperature and power profiles. These depend on the cross-field transport processes in the SOL, but since perpendicular particle and thermal transport in the SOL are anomalously high, λ_n, λ_T and λ_P must be determined experimentally: in current experiments the SOL decay lengths are typically 1 cm or less at the plasma midplane. Under certain simplifying assumptions, there is a straightforward relationship between the temperature and power decay lengths (e.g. [97P1]),

$$\lambda_P = \frac{2}{7}\lambda_T \ , \tag{6.48}$$

indicating the importance of cross-field thermal transport processes in determining the power decay length. Equation (6.48) also illustrates that anomalous transport in the SOL is beneficial, since it increases the power decay length and reduces the peak heat flux to the power handling surfaces.

As power and particles flow along field lines into the divertor region (taken to be the region below the X-point in Fig. 6.10), a variety of processes can modify the power and the particle fluxes which arrive at the surface of the targets. In considering these aspects of the plasma-surface interaction, details of the "sheath", the narrow interface between the plasma and the solid surface, will be neglected, but treatments of this region can be found, for example, in [90S1, 97W1, 00S2].

The production of impurities and the subsequent influence which they have on the core and edge plasma behavior is a central aspect of plasma-surface interaction studies. For example, core contamination by low-Z materials such as beryllium or carbon is tolerable at concentrations of 1…2 % of the electron density, but for high-Z materials such as tungsten the contamination level must be several orders of magnitude lower. Impurities arise from two principal sources, "sputtering" from the divertor targets and walls of the chamber, due to ion and neutral impact, and external seeding of selected impurities to enhance the fraction of power lost via radiation. The latter is an effective means of reducing the power flowing to the targets. Sputtering, the removal of atoms from a solid surface by interaction with the plasma particles, is divided into two general processes: "physical sputtering" involves the removal of an atom from the solid lattice by the transfer of momentum due to the impact of ions or neutrals, while "chemical sputtering" applies to the process in which a chemical bond is formed between hydrogen isotopes and carbon, or between oxygen and carbon, resulting in the release of the carbon from the surface in the form of a hydrocarbon or CO. Additional sources of impurity contamination include desorption of volatile impurities, such as water vapor or CO, by plasma particles or surface heating, local melting or evaporation of the surface by overheating, and arcing between the plasma and the solid surface ("unipolar arcing").

Interactions with neutrals in the divertor region can make important contributions to the transport of energy and momentum, and their role becomes increasingly significant as the divertor density rises and the temperature falls. The principal sources of neutrals in the divertor are "recycling", the reflection or desorption of neutralized plasma ions from the divertor target, and "recombination" of ions and electrons,

though the latter process is important only at low divertor plasma temperatures, ≈ 1 eV. The main plasma-neutral interactions involving atomic hydrogen isotopes are excitation, ionization, charge exchange and radiative recombination. Excitation and ionization are produced by electron-neutral collisions and both lead to cooling of the electrons. Charge exchange reactions constitute an important channel through which ion energy and momentum is dissipated, while radiative recombination is a key process by which plasma kinetic energy is converted to radiation in the very low temperature regime characterized by "detachment" (see below).

Analysis of the power handling problem for reactor scale plasmas (e.g. [99I1]) indicates that power fluxes to the divertor targets can be reduced to an acceptable level only if a substantial fraction of the exhaust power is lost by impurity radiation, which leads to a redistribution of the power in an approximately uniform manner over a large fraction of the first wall. Intrinsic impurities can contribute to this scenario, but if materials such as tungsten are utilized for the divertor targets, an additional source of radiating impurities, such as neon or argon, will be required (see Sect. 6.6.3).

The use of impurity radiation to reduce the power loading of the divertor target is designed to promote "detachment" of the divertor (e.g. [97P1, 99I1]), in which energy and momentum are transported to the PFCs entirely via radiation and neutral particles. In the more usual operating regime for the divertor plasma, the "attached" regime, the electron temperature in the divertor is everywhere above 10 eV and the total plasma pressure (static plus dynamic) is constant along the field lines from the plasma midplane to the target plates. If the divertor temperature in front of the target plate can be reduced to ≈ 5 eV, several processes combine to initiate detachment: the fraction of power radiated by impurities increases, since line radiation is more efficient at lower temperature for the low- to medium-Z impurities in question; ion-neutral interactions, such as charge exchange, transfer energy and momentum from the ions to the neutrals, leading, in particular, to radial transport of momentum; and, as the temperature falls to 1…2 eV, recombination of ions and electrons makes a significant contribution to the radiated power loss and the dissipation of plasma pressure. Energy transport to the targets and other PFCs then takes the form of volume radiation losses and neutral particle recycling. In this regime, radiation, principally in the form of impurity line radiation and hydrogen recombination, can account for almost 100 % of the power. Since gradients exist both parallel and perpendicular to the field lines in the divertor, the degree to which the plasma is detached can vary radially across the strike region in front of the targets, a scenario which is referred to as "partial detachment".

The selection of suitable materials for plasma facing components, in particular for divertor targets, is a key question for magnetic fusion research. The principal criteria are: ability to tolerate high heat fluxes under steady-state and transient conditions; high thermal conductivity; low erosion rate, which relates both to an acceptable operational lifetime and minimal contamination of the plasma core; low affinity for hydrogen isotopes, to minimize tritium retention in the torus; mechanical strength; and low neutron activation. Power handling capability is complicated by transient events such as disruptions and ELMs, since the energies involved at the reactor scale could produce melting and evaporation of the surface of the divertor targets, which would limit the target lifetime (e.g. [97P2]). Low-Z materials are attractive for PFCs in present tokamaks, where PFC lifetime is not an issue. Carbon, in the form of graphite or carbon fibre composites (CFC), is the most favored material, as it combines many of the necessary properties and permits considerable operational flexibility. However, evidence from D-T experiments in JET [98G1] and TFTR [97S3] indicates that "codeposition" of tritium with redeposited carbon causes the retention of significant levels of tritium in the vacuum vessel, which is problematic in the reactor context. Beryllium is an alternative low-Z material which has several attractive features, and which has been investigated in JET (e.g. [97C1]). However, it melts at relatively low temperatures, 1270 °C, and the transient power loads which could be expected at the reactor scale are likely to lead to surface melting. In a reactor, therefore, high-Z materials such as tungsten may be a more appropriate solution for PFCs. If the divertor temperature can be held low enough so that ions incident at the surface are below the physical sputtering threshold (requiring a divertor temperature below 20 eV in the case of tungsten [95W1]), the sputtering rate would essentially be zero and an acceptable target lifetime could be achieved. Moreover, tritium retention is not expected to be a significant problem. Tungsten divertor targets have been studied in ASDEX Upgrade [97N1] and, although this experiment was not able to explore all aspects relevant to a reactor, acceptable results in terms of both plasma and divertor target performance were obtained.

6.6.3 Divertor experiments

The rationale for the use of the poloidal divertor configuration (Fig. 6.10) is that the plasma-wall interactions are removed from the immediate proximity of the plasma edge and it is expected theoretically that particle flows in the divertor plasma and SOL will reduce the fraction of impurities which penetrates to the main plasma. In addition, it should be possible to approach (complete or partial) divertor detachment, which could solve both the power handling and impurity production problems. Finally, it has been shown that the configuration allows efficient removal of helium from the plasma. The trend towards poloidal divertor tokamaks has been further accelerated by the experimental discovery in ASDEX that access to the H-mode confinement regime is possible (H-mode operation is very difficult in limiter configurations). The majority of experiments have explored single null divertor plasmas and since this geometry is favored for the proposed international burning plasma experiment, ITER (Sect. 6.10), the discussion here is restricted to observations relating to this configuration.

A central aim in current divertor experiments has been the demonstration of plasma regimes in which power is dissipated by volumetric losses. Experiments in L-mode plasmas using hydrogen gas-puffing to raise the plasma density, and ultimately cool the divertor plasma, have demonstrated fully detached plasmas and have confirmed several aspects of plasma behavior associated with detachment (e.g. [97P1, 99I1]). Figure 6.11 illustrates the radial profiles of pressure and electron temperature in the SOL at the plasma midplane and at the divertor target for a sequence of time slices as the density is raised and detachment is approached in the Alcator C-Mod tokamak, located in the US [95L2].

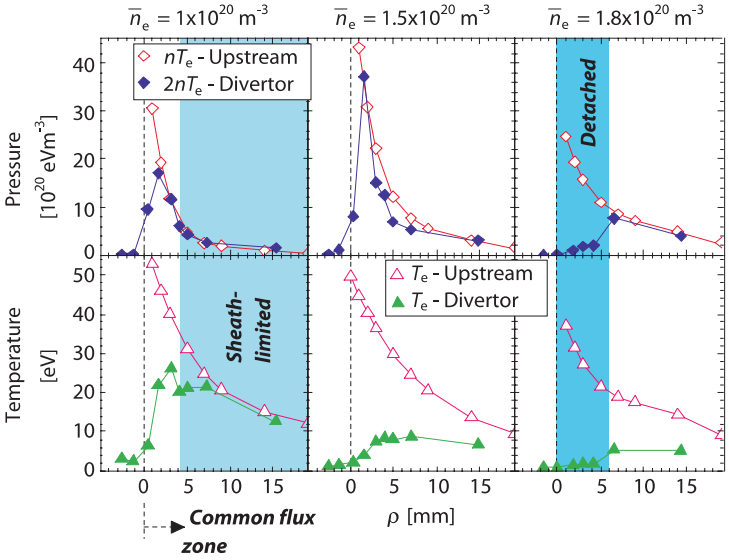

Fig. 6.11. A sequence of radial pressure and temperature profiles measured in the plasma midplane SOL and at the divertor target (and mapped to the midplane flux surfaces) in the Alcator C-Mod tokamak as the plasma density is increased. The right hand panel illustrates the significant difference between the midplane and divertor pressures, together with the very low divertor electron temperature, in the detached phase [95L2].

In detached divertor experiments, a significant fraction of the radiation is emitted from a "mantle" just inside the separatrix. In many cases, the divertor radiation concentrates near to the X-point as detachment is approached and can eventually form a "MARFE" (multifaceted asymmetric radiation from the edge). The MARFE, which was first observed in limiter tokamaks [84L1], where it forms a component of the radiation precursor to high density disruptions, is a poloidally localized, but toroidally symmetric, region of high density, cold plasma which radiates copiously. It results from a radiation instability related to the fact that, for many impurities, line radiation increases with decreasing electron temperature in the region below ≈ 50 eV. The phenomenon is of general importance for highly radiating plasma scenarios in tokamaks, since it sets an instability limit to the detachment process.

In H-mode plasmas, impurity seeding, using gases such as neon, argon or nitrogen, is generally required in combination with hydrogen puffing to achieve detachment. However, with few exceptions (e.g. the CDH-mode in ASDEX Upgrade [95G1] – Sect. 6.4.2), the confinement degrades as the density and radiated power fraction rise. In addition, the level of impurity contamination associated with impurity

seeding in present devices is unacceptably high. Nevertheless, analysis of highly radiating regimes in both divertor and limiter tokamaks has concluded that the expected level of impurity contamination in reactor scale plasmas should be acceptable [97M1].

Modeling and experiments have identified two specific features of divertor geometry which may influence plasma behavior: the use of vertical, rather than horizontal, divertor targets (as in Fig. 6.10) and the use of tight "baffling" of the divertor, i.e. the use of tight fitting sidewalls to the divertor to which the plasma geometry can be closely matched. The use of vertical targets promotes the occurrence of detachment in the vicinity of the separatrix, where the heat flux is highest, while baffling of the divertor relates to the concept of divertor "closure", defined quantitatively by the compression ratio,

$$C = \frac{n_{\mathrm{mol,div}}}{n_{\mathrm{mol,mid}}} \ , \tag{6.49}$$

where $n_{\mathrm{mol,div}}$ and $n_{\mathrm{mol,mid}}$ are the densities of molecular hydrogen in the divertor and main chamber respectively. High compression ratios imply that neutrals are efficiently trapped in the divertor. Improved baffling has been found to increase the compression ratio in tokamak plasmas, with factors of ≈ 100 being achieved, leading to higher particle exhaust rates, which is beneficial for helium exhaust.

Requirements for the exhaust of helium ash from reactor plasmas were introduced in Sect. 6.3.2. A substantial database relating to helium exhaust in limiter and divertor configurations exists (e.g. [97H1]) showing that, in L-modes and ELMy H-modes, helium transport in the main plasma is not a limiting factor in the removal of helium and that helium exhaust rates are determined by the neutral helium pressure in the divertor, together with the effective pumping speed. Several experiments have achieved values of $\tau^*_{\mathrm{He}} / \tau_E \approx 5$, well within the requirements for a power plant, but have found that the helium concentration is lower in the divertor than in the main plasma. An "enrichment factor" is defined by

$$\eta_{\mathrm{He}} = \frac{n_{\mathrm{He,gas}}}{2 n_{\mathrm{H,mol}}} \frac{n_{\mathrm{e,s}}}{n_{\mathrm{He,s}}} \ , \tag{6.50}$$

where $n_{\mathrm{He,gas}}$ is the neutral helium density in the divertor (outside of the divertor strike zones), $n_{\mathrm{H,mol}}$ is the hydrogen molecular density in this region, $n_{\mathrm{He,s}}$ is the helium ion density at the midplane separatrix and $n_{\mathrm{e,s}}$ is the midplane separatrix electron density. Studies of ELMy H-modes in ASDEX Upgrade have shown that the enrichment factor falls with increasing divertor neutral pressure to values of ≈ 0.2 [97B2], which are nevertheless acceptable for a reactor.

6.7 Steady-state operation

Steady-state operation of a tokamak reactor could have a significant influence on the economic viability of fusion power (e.g. [93K1, 94G1, 95G2, 99N1]). However, the pulse length of the largest tokamak experiments is typically restricted to a few tens of seconds, since the plasma current is driven inductively. Provision of a non-inductive current drive capability relies on exploiting current driven by the bootstrap mechanism (Sect. 6.2.4) and by auxiliary heating systems (Sect. 6.3.1). High bootstrap current fractions (≈ 80 %) can be achieved under appropriate conditions, as illustrated in Fig. 6.4, while lower hybrid current drive (LHCD) has been used to produce fully non-inductive plasma pulses lasting for 2 hours at 20 kA in the TRIAM-1M tokamak in Japan [97I1] and for 120 s at 800 kA in Tore Supra, located in France [97S4]. Nevertheless, at the current drive efficiencies expected in tokamak power plants, several hundred megawatts of auxiliary heating power would be required to achieve full current drive by external means, leading to an uneconomic burden of recirculating power. The concept for steady-state tokamak operation favored at present, therefore, involves a substantial bootstrap current contribution, probably above 70 % of the plasma current, with the remaining fraction of the current driven by auxiliary heating systems. If the current drive efficiency of auxiliary heating systems extrapolates as predicted from existing experiments (see discussion below), an additional heating power of less than 100 MW would be required in a tokamak power plant. This is fundamental for the viability of steady-state operation in toka-

mak reactors, since the overall thermal power gain of the reactor core is expected to be determined by the current drive requirement, rather than by confinement constraints.

Many technical design features of tokamak power plants will be similar in steady-state and pulsed cases, since, at the reactor scale, plasma pulses may last for several hours. In terms of the demands on magnet technology, power handling, tritium breeding etc., a pulse of several hours effectively implies steady-state operation (though a true steady-state device might benefit from a reduction in the size of the central solenoid and associated PF power and cryogenic requirements [93K1]). The principal technological benefits of steady-state operation would include the absence of thermal and electromagnetic cycling stresses in the in-vessel structures and magnets (which might otherwise limit the maximum toroidal field [97N2]), and the elimination of a system for smoothing the electrical output power in the inter-pulse period.

Physics differences between the requirements of pulsed and steady-state operation are clearer. In particular, while scenarios with pulsed operation typically seek to maximize the plasma current, so as to increase the energy confinement time (see (6.43)), steady-state operation imposes the additional constraint that the plasma current must be fully maintained by the sum of the bootstrap and external current drive sources. In addition, (6.22) indicates that high bootstrap current fractions ($f_{bs} = I_{bs}/I_p$) imply operation at high-β_p (further favoring lower I_p). If (6.22) is recast in the form

$$f_{bs} \approx \varepsilon^{-0.5} h(\kappa) \beta_N q_c \ , \tag{6.51}$$

where $h(\kappa)$ is an increasing function of elongation, it is clear that steady-state operation is favored by operation at large aspect ratio, elongation, normalized β and safety factor. However, as discussed in Sects. 6.9 and 6.10, operation at low aspect ratio (i.e. in "spherical tokamaks") has advantages in terms of the achievable values of κ and β_N, so that (6.51) does not unambiguously identify an optimal direction in parameter space for the development of a steady-state tokamak.

Experimental studies of plasma operating regimes having negative central shear and internal transport barriers (Sect. 6.4.2), together with theoretical analyses aimed at optimizing the fusion performance of such plasmas (e.g. [94K1, 95T1]), have highlighted the concept of an "advanced tokamak scenario" (e.g. [94G1, 97T1]) which has greater potential for steady-state operation than conventional confinement regimes (e.g. L- and H-modes). The essential physics embodied in the advanced tokamak concept is the exploitation of plasma shaping, particularly triangularity, and profile control to establish NCS plasmas (Sect. 6.4.2), which have been demonstrated theoretically and experimentally to have the potential for access to high values of β_N (theoretical analyses suggest $\beta_N > 5$).

Negative central shear can improve plasma stability in several ways. Firstly, the NCS q-profile invariably has a minimum q value greater than unity, eliminating the drive for the $m = 1$, $n = 1$ mode responsible for sawteeth. NTMs are also stable in the NCS region and such q-profiles provide access to an improved mhd stability regime, so-called "second stability" [81G1], which suppresses further potential β-limiting instabilities in the plasma core. Finally, the broader current profile promotes improved mhd stability through the phenomenon of "wall stabilization" of ideal kink modes, although measures must be taken to deal with the RWM (Sect. 6.5.5). A particularly attractive aspect of the NCS regime is that, if high values of β_N can be achieved, the substantial bootstrap current which develops will align itself closely to the form required to maintain the negative shear region in the core: the bootstrap current depends on the presence of trapped particles and is driven by the pressure gradient. Both of these contributions reach their maximum at some distance from the plasma axis, so that the bootstrap current develops a "naturally" hollow profile, as illustrated in Fig. 6.12. Realization of the full benefit of the NCS regime, however, relies on careful design and control of the plasma current, pressure and rotation profiles in order to avoid additional sources of instability (e.g. [97T1]). Improvements in plasma control will therefore be required to sustain true steady-state operation in tokamaks [99M1, 00J1, 00L1].

NCS plasmas also provide the basic conditions in which ITBs can develop, leading to confinement enhancement above the normal H-mode level. For example, it has been shown that reduced or negative magnetic shear suppresses several microinstabilities which can contribute to anomalous transport. Control of power and particle exhaust in NCS plasmas is, however, at an early stage, since such plasmas are generally established at densities well below the Greenwald value. Scenarios in which the density is raised to reactor relevant values must therefore be developed in the future, both to produce adequate fusion power

and to establish edge and divertor conditions which satisfy the requirements for power exhaust and the extraction of helium discussed in Sect. 6.6.

In present experiments the NCS regime is transient, lasting for several seconds, since it is established by careful tailoring of the initial plasma current ramp-up and heating scenario and so exploits the delay which occurs as the plasma current profile relaxes resistively towards its equilibrium distribution. Progress has been made towards a quasi-steady-state regime in several devices, including Tore Supra [96L1], JT-60U [00O1], DIII-D [01A1] and ASDEX Upgrade [99G3], but the attainment of true steady-state conditions will require the use of non-inductive current drive methods to control the local current density and sustain an appropriate current profile for maintenance of both the ITB and mhd stability.

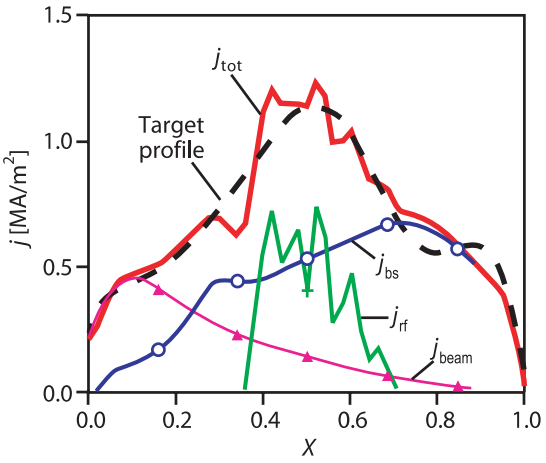

Fig. 6.12. A numerical analysis of the current density profile for an optimized negative central shear scenario in the DIII-D tokamak, illustrating the contributions to the proposed fully non-inductive current profile: the target profile is shown as the heavy dashed line, while the sum of the calculated non-inductive components is shown by the heavy solid line. Note, in particular, the hollow form of the bootstrap current contribution, j_{bs} [95T1].

6.8 Energetic particle physics

6.8.1 Energetic particle confinement

In a D-T fusion reactor, 3.5 MeV α-particles will provide the dominant source of plasma heating. It is therefore essential that they are well confined so that they transfer their energy efficiently to the background plasma. This is equally true for energetic particle populations produced by heating and current drive systems. Although it is only in recent years that initial D-T experiments in the TFTR and JET tokamaks have allowed the behavior of α-particles to be studied directly (e.g. [98H2, 99K1]), energetic ions produced by NBI and ICRF, as well as fusion products resulting from D-D and D-^{3}He reactions, had already provided considerable insight into the confinement of energetic particles and their interactions with the thermal plasma. Since the particles in question typically have energies which are a factor of $\approx 10^2$ greater than the thermal ions, confinement of the particle orbits within the closed flux surfaces is itself an issue. The key parameter is the average displacement of the trapped particle (banana) orbit from the magnetic surface, which, as defined in (6.15), depends on the Larmor radius in the poloidal field. This provides a straightforward estimate for the minimum plasma current required to confine α-particles, which turns out to be ≈ 3 MA (e.g. [94S1]). Since this is at least a factor of 3 less than the plasma current in the majority of power plant studies (e.g. [94S1, 97N2]), this criterion is not a problem at the reactor scale, though it must be considered in all but the largest of the existing tokamaks.

Under some conditions, for example in low density plasmas with high power auxiliary heating (NBI or ICRF), or in a reactor at high temperature (≈ 20…30 keV), energetic ions can contribute a significant fraction (≈ 20 %) of the plasma energy. However, the high particle energy means that the particle density is no more than a few percent of the electron density. Collisions between the energetic ions can therefore be neglected and the principle factors affecting their slowing down and transport are those involving collisions with the background plasma, interactions with microinstabilities responsible for anomalous transport, toroidal field ripple effects (discussed below) and interactions with large scale mhd instabilities

(Sect. 6.8.2). The classical processes by which energetic particles transfer energy to the background plasma, summarized in (6.23) to (6.25), have been tested in many experiments using energetic ions produced by heating systems. These measurements have confirmed that such populations slow down and transfer their energy to the thermal plasma at the predicted rate [94H1], as illustrated in Fig. 6.13. Additional supporting evidence is provided by D-T experiments in TFTR [96T1] and JET [98T2], where, within experimental errors, the level of electron heating by α-particles was as expected. Energetic ions also suffer a significantly lower level of anomalous transport due to turbulence than thermal particles: in mhd-quiescent discharges, the derived rate of radial diffusion for energetic particles is more than an order of magnitude lower than for thermal ions.

The situation with respect to energetic particle confinement would therefore be entirely satisfactory were it not for the consequences of toroidal field (TF) ripple and large scale mhd instabilities. TF ripple is the regular perturbation of the toroidal field which occurs due to the finite number (≈ 20) of toroidal field coils. The amplitude of the TF ripple is defined by

$$\delta_{\mathrm{TF}} = \frac{B_{\max} - B_{\min}}{B_{\max} + B_{\min}} \ , \tag{6.52}$$

where $B_{\max}$ and $B_{\min}$ are respectively the maximum and minimum values of the toroidal field encountered when following a toroidal circle around the torus. $B_{\max}$ occurs under each toroidal field coil, while $B_{\min}$ occurs midway between two coils. The level of TF ripple depends on several factors, but principally the number of TF coils and the torus aspect ratio. It is a maximum on the outboard edge of plasma, where it is generally ≈ 1 %, and falls rapidly towards the high field side of the torus – in the plasma center it is usually several orders of magnitude smaller than at the outboard midplane.

The orbits of trapped energetic particles can be influenced in several subtle ways by the ripple perturbation, leading to anomalously rapid energetic particle losses. The theory of such orbit disturbances is well developed and has been confirmed quantitatively by extensive comparisons with experimental observations (e.g. [94H1, 99I1]). Although the resultant energetic particle losses may only amount to several percent, which is not harmful to plasma performance, the spatially localized nature of the losses can produce significant damage to the first wall. Moreover, energetic particles intersect the walls at low angles of incidence, further localizing the power deposition. This is therefore an important issue for the design of burning plasma experiments. It is of particular concern for the NCS scenarios favored for steady-state operation, since the reduced poloidal field strength in the plasma center leads to larger banana orbits, which are more vulnerable to ripple losses. However, the good agreement between experimental measurements and theory in this area should allow satisfactory TF coil designs to be developed which limit losses to the walls to within acceptable bounds.

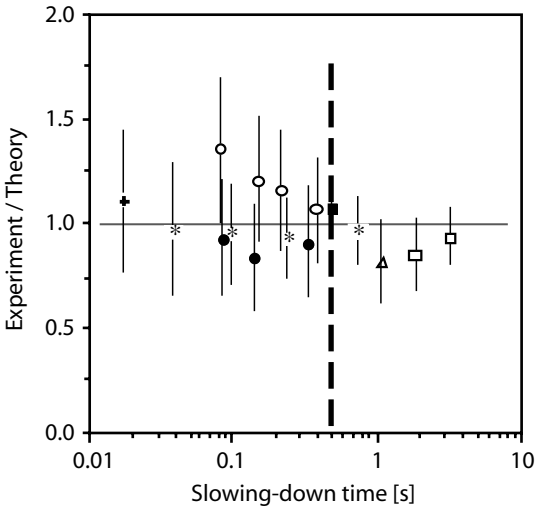

Fig. 6.13. Ratio of the measured slowing-down time of energetic particle populations to that predicted by classical slowing-down theory for several tokamak experiments. The particle energies range from 30 keV deuterons to 3.5 MeV α-particles [94H1].

6.8.2 Energetic particle interactions with mhd instabilities

Energetic particles influence the stability properties of various forms of mhd activity, and mhd instabilities can, in turn, influence the confinement of the energetic particles and have the potential to produce additional losses. The long sawtooth-free periods observed in several tokamak experiments [88C2] are perhaps the clearest examples in which energetic particles stabilize an mhd instability. The favored explanation is that the trapped particle component of the high energy population suppresses the growth of the $m = 1$, $n = 1$ mode responsible for sawteeth. A model developed to investigate the influence of α-particles in D-T plasmas [96P1] predicts that the α-particle stabilization of sawteeth could produce sawtooth-free periods lasting for tens of seconds. Although the sawtooth collapse can redistribute a fraction of the energetic particle population from the plasma center to regions outside the $q = 1$ surface, the effect is not considered to be critical for the power balance in a burning plasma.

Energetic particles can also excite $m = 1$, $n = 1$ modes when the trapped particle drift precession frequency (e.g. [94H1]) matches the natural frequency of the mode. This form of instability, known as "fishbones" [83M1], as a result of the characteristic bursting signal observed in the magnetic fluctuations as the modes grow and then decay, has been observed in many experiments. Fishbones can cause large losses of fast particles as a result of the resonant interaction (e.g. [94H1, 99I1]), but in larger tokamaks they merely result in internal spatial redistributions of the energetic particles. They might be excited by α-particles in burning plasmas if the β of the α-population is high enough.

Shear Alfvén waves (e.g. [97W1]) are a general class of plasma waves which, in toroidal geometry, form a series of continuous frequency bands. Within these bands the waves are strongly damped, but the bands are separated by gaps within which a series of discrete "Alfvén eigenmodes" (AE) can exist. These eigenmodes can be driven unstable by particles whose velocity is greater than V_A, see (6.44) [86C1, 89F1], a condition which will be satisfied by 3.5 MeV α-particles in burning plasmas. In a tokamak plasma, several gaps arise from toroidicity, ellipticity and triangularity (non-circularity), and the eigenmodes which can be excited within these gaps are referred to as TAEs, EAEs and NAEs respectively. Lower frequency modes associated with finite compressibility (BAEs, or beta-induced AEs), or intrinsically associated with the presence of an energetic particle population ("energetic particle modes", or EPMs) have also been identified (e.g. [99W1, 99I1]). For a given q-surface, an Alfvén frequency,

$$\omega_A \approx \frac{V_A}{qR} \ , \tag{6.53}$$

can be defined, and the centers of the TAE, EAE, NAE gaps then correspond approximately to $\omega_A/2$, ω_A and $3\omega_A/2$. Free energy available in the energetic particle pressure gradient is responsible for the instability drive for the modes, but several damping mechanisms exist, so that the calculation of the stability of the modes is complex.

Experiments have confirmed that energetic ions produced by neutral beam injection can destabilize AEs when the toroidal field is reduced to bring V_A into the velocity range which matches the available ion energies (80…100 keV) [91W1, 91H1]. It has been shown that the modes, in particular TAEs, can produce substantial losses of energetic ions, with up to 70 % of beam injected ions being lost in TFTR and DIII-D (e.g. [99W1]). Studies of TAEs driven unstable by α-particles have been attempted in D-T experiments in TFTR and JET (e.g. [98H2, 99K1]). In the latter case, no evidence for α-particle driven Alfvén eigenmodes was obtained, while in TFTR α-driven modes were produced only in plasmas with weak central shear and high $q(0)$ in the phase following switch-off of the NBI heating. This confirmed predictions that the stability threshold is sensitive to the q-profile and that damping due to thermal and energetic plasma components is important. No α-particle losses resulted from the α-driven TAEs.

6.9 Tokamak experiments

6.9.1 Present status

The tokamak fusion program is centered around approximately 20 major facilities, plus many smaller devices. Table 6.2 lists the principal parameters of the largest devices, taken here to be those having a plasma current in excess of 0.5 MA. The majority of the largest devices now employ the poloidal divertor or X-point configuration (although spherical tokamaks can be operated in a limiter or divertor configuration, the tight aspect ratio favors the formation of a natural X-point equilibrium). Divertor and X-point configurations correspond to essentially the same plasma equilibrium, but a distinction is often made, depending on whether the device incorporates specialized internal structures to isolate the divertor plasma, at least to some extent, from the main plasma, but this distinction will be neglected here. Note that all but one of the devices listed in the table are based on copper TF and PF magnet systems. The exception is Tore Supra, which utilizes a TF magnet fabricated from NbTi superconductor, a feature which has also been tested in several smaller tokamaks.

The most significant development in the design of divertor tokamaks has been the focus on increasingly sophisticated divertor geometries which has occurred during the last decade. Incorporating major elements of the divertor geometry proposed for ITER, such as vertical divertor targets, close baffling and cryopumps, these "closed" divertor geometries have also accommodated studies of various power handling materials, such as beryllium (JET), molybdenum (Alcator C-Mod) and tungsten (ASDEX Upgrade), in addition to the more conventional carbon. Building on experimental observations that increased plasma shaping is beneficial in terms of plasma confinement and stability, divertor geometries have been adapted to accept more highly triangular plasmas. Overall, there has been substantial progress in the control of plasma-wall interactions, with the emphasis on the development of a self-consistent scenario for reactor-grade experiments which combines satisfactory core confinement and stability properties with edge and divertor plasma parameters required to meet engineering constraints on PFC power handling and the demands of helium ash exhaust ("core-edge integration").

Table 6.2. Principal parameters of the largest tokamak experiments.

Device	Location	Config.	R [m], a [m]	I_p [MA]	B_ϕ [T]	P_{aux} [MW]
Alcator C-Mod	USA	Divertor	0.67, 0.22	1.5	8.1	7
ASDEX Upgrade	Germany	Divertor	1.65, 0.5	1.2	2.0	22
DIII-D	USA	Divertor	1.67, 0.67	3.0	2.1	23
FTU	Italy	Limiter	0.93, 0.30	1.6	8.0	5.3
GLOBUS-M	Russia	Spherical	0.36, 0.24	0.5	0.65	3
JET	EU (UK)	Divertor	3.0, 1.0	6 [1])	3.8	35
JT-60U	Japan	Divertor	3.4, 1.1	5	4.5	40
MAST	UK	Spherical	0.75, 0.55	2	0.6	6.5
NSTX	USA	Spherical	0.85, 0.68	1	0.6	11
TCV	Switzerland	Divertor	0.88, 0.24	1	1.54	4.2
TEXTOR	Germany	Limiter/DED	1.75, 0.48	0.8	3.0	9
TFTR [2])	USA	Limiter	2.52, 0.87	3	5.9	40
Tore Supra	France	Limiter	2.4, 0.79	2.1	4.25	15
T-10	Russia	Limiter	1.5, 0.37	0.68	4.5	2

[1]) JET achieved 7 MA in limiter operation.

[2]) TFTR ceased operation in April 1997.

Limiter tokamaks have experimented with particle control via pumping (e.g. TEXTOR and Tore Supra) and a major limiter facility is being commissioned in Tore Supra. Denoted "CIEL" [98G2], this actively cooled toroidal pumped limiter is designed to handle plasmas with 25 MW of input power for up to 1000 s, allowing the first studies of high temperature tokamak plasmas which are in steady-state with respect to resistive diffusion and plasma-wall interactions. This presages the technology required for long pulse burning plasma experiments. In contrast, plasma facing components in all other devices are "inertially cooled", i.e. they are cooled by conduction to the supporting structure and by radiation, since plasma pulse durations typically range from fractions of a second to some tens of seconds. Tore Supra has also investigated the "Ergodic Divertor" (ED) geometry [96G1], in which a region of "ergodized" magnetic field (i.e. the magnetic field no longer consists of nested closed surfaces) is established in the edge of a limiter plasma by means of a series of localized coils. Amongst other benefits, the ED configuration is more effective in shielding the plasma against impurities than a simple limiter. A development of this concept, the "Dynamic Ergodic Divertor" (DED) [97F1], which allows the structure of the ergodized layer to be varied rapidly in time, is being studied in TEXTOR.

The last decade has also seen the development of the "spherical tokamak" (ST) concept [86P1]. In spherical tokamaks, the central core, containing the solenoid and inner leg of the toroidal field coil, is made extremely compact, so that a torus with very small aspect ratio (typically $R/a \approx 1.3$) can be constructed, as illustrated in Fig. 6.14. The advantages of the ST are associated fundamentally with configurational and stability aspects of the resultant plasma equilibrium. For example, due to the low aspect ratio, ST equilibria exhibit high "natural" elongation and triangularity. These factors allow operation at high plasma current, favoring high energy confinement, at modest toroidal field while maintaining $q_{95} \approx 3$. As a consequence, the normalized current, $I_N = I_p(\mathrm{MA})/a(\mathrm{m})B_\phi(\mathrm{T})$, is large, and high values of β can be attained at acceptable values of β_N, as exemplified by plasmas with $\beta \approx 40$ % and $\beta_N \approx 6$ obtained in the small START device in the UK [97S1]. Theoretical studies suggest that values of $\beta_N \approx 8$ might be achievable [97M2]. Key issues for the further development of the ST concept include confirmation of the predicted stability advantages in hot collisionless plasmas, the achievement of substantial pressure driven

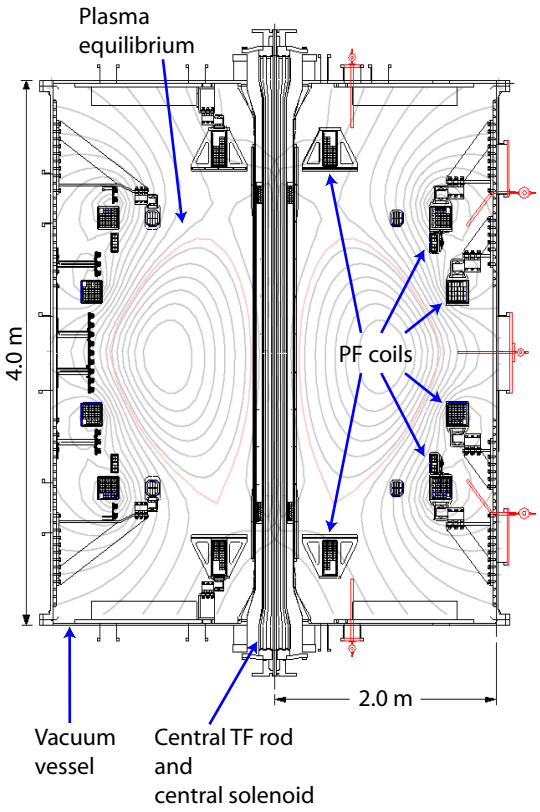

Fig. 6.14. Cutaway view of the MAST spherical tokamak assembly, indicating the main elements.

currents, and the demonstration of a satisfactory power handling scenario in the constrained divertor geometry which characterizes low aspect ratio configurations. As indicated in Table 6.2, two STs, MAST and NSTX, with plasma currents in the MA range and plasma dimensions comparable to conventional medium sized tokamaks, are now studying these questions.

Over the past thirty years, the increases in plasma dimensions, current, toroidal field and auxiliary heating power, together with the discovery of regimes of enhanced confinement, have been responsible for an improvement of several orders of magnitude in fusion performance. Since virtually all experiments operate in hydrogen or deuterium, to minimize neutron production and the resultant activation of the tokamak structure, this has not been directly reflected in the fusion power production (but see Sect. 6.9.2). However, the "fusion triple product", $n_H(0)T_i(0)\tau_E$, where $n_H(0)$ is the central "fuel" density (i.e. hydrogen or deuterium in current devices) and τ_E is the thermal energy confinement time, is an accepted figure of merit for fusion performance. Under certain simplifying assumptions relating to the D-T fusion cross-section and the plasma profiles (e.g. [97W1]), the ignition parameter, C_{DT}, can be expressed as,

$$C_{DT} = \frac{Q_{DT}}{Q_{DT}+5} = \frac{P_\alpha}{P_{loss}} \approx 2\times10^{-22} n_H(0)T_i(0)\tau_E \quad (T_i(0) \text{ in keV}) \ , \tag{6.54}$$

where P_α is the α-heating power in D-T plasmas and P_{loss} the power lost via conduction, convection and radiation. $C_{DT} = 1$, equivalent to $n_H(0)T_i(0)\tau_E \approx 5 \times 10^{21}$ m^{-3}keVs, corresponds to ignition.

The progress in fusion performance of existing devices is illustrated in Fig. 6.15, where the highest values of fusion triple product obtained in a range of modern tokamaks during the last thirty years is plotted against the central ion temperature. The three large tokamaks, JET, JT-60U and TFTR, have reached values which are within a factor of 5 of that required for ignition and are equivalent to thermonuclear fusion gains of unity, $Q_{DT} = 1$. This is commonly referred to as "scientific breakeven", since the plasma

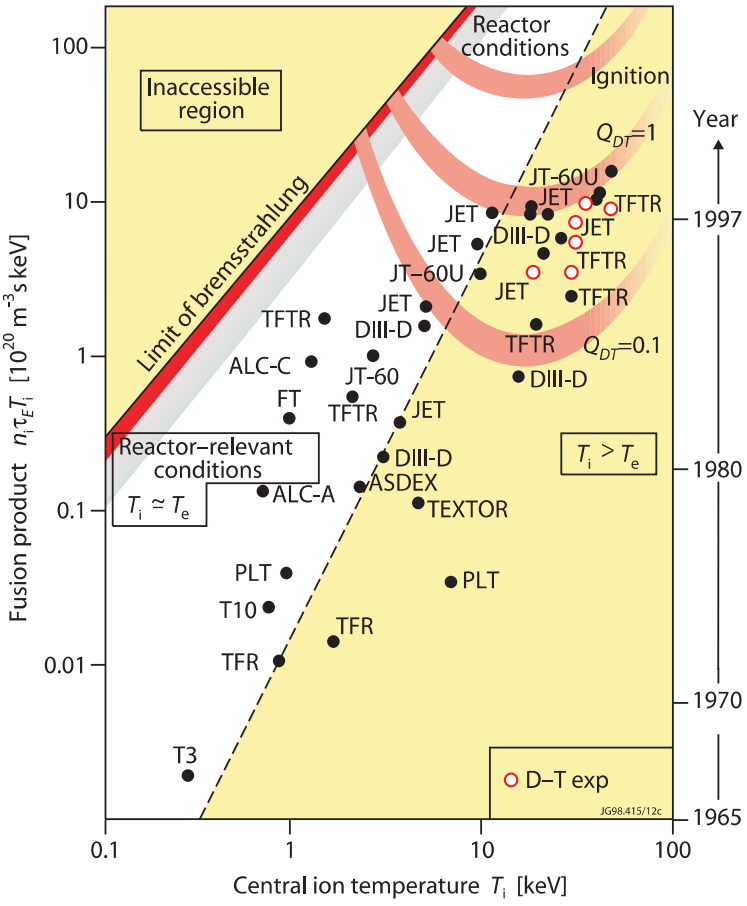

Fig. 6.15. Representative values of the fusion triple product, $n_i\tau_E T_i$, plotted against the central ion temperature, T_i, for a range of modern tokamak experiments. Curves corresponding to several values of the thermonuclear power gain, Q_{DT}, are indicated. Note that several of the points derive from the D-T experiments discussed in Sect. 6.9.2.

parameters are such that, if D-T fuel were used, the fusion power would equal the power deposited in the plasma. Note that the highest $n_H(0)T_i(0)\tau_E$ values are typically attained under transient conditions, lasting only ≈ 1 s, and that a significant fraction of these are obtained in the "hot-ion" regime, where the ions are effectively decoupled from the electrons and the central ion temperature may be a factor of 3 greater than the central electron temperature. The region of parameter space encompassing "Reactor-relevant conditions", for which $T_i(0) \approx T_e(0)$, is indicated.

6.9.2 Deuterium-tritium experiments

The use of a deuterium-tritium mixture in tokamak experiments requires several precautions. In particular, the 14.1 MeV neutrons produced by the D-T reactions require substantial concrete shielding around the experiment to protect personnel. They also induce significant activation of the tokamak structure, which necessitates the use of remote handling techniques for in-vessel maintenance and installation work following D-T operation. In addition, tritium is radioactive and some fraction is retained in the torus, necessitating a more sophisticated approach to vacuum confinement and gas-handling ("double containment"), to avoid releases to the atmosphere. There are, moreover, strict regulatory controls on the handling of tritium. Nevertheless, both JET and TFTR were designed with the capability to carry out experiments in D-T plasmas, since this is viewed as a necessary confirmation of key aspects of fusion physics before the construction of the next generation of burning plasma devices which will lay the basis for the design of a demonstration tokamak reactor.

A principal motivation for performing D-T experiments in the present generation of tokamaks is that D-T experiments can provide confirmation that the interpretation of fusion performance summarized in Fig. 6.15 is correct and that the expected level of thermonuclear fusion power production can be achieved. Initial studies of D-T plasma performance were conducted in late 1991 in the JET "preliminary tritium experiment" (PTE), which was restricted to maximum tritium concentrations of 11 % to minimize activation of the vessel structure [92J1]. Subsequently, more extensive experiments, with 50:50 mixtures of deuterium and tritium, were carried out in TFTR in the period 1993…1996 (e.g. [98H2]) and in JET in 1997, referred to as DTE1 (e.g. [99K1, 99J1]). Fusion power production increased from 1.7 MW in the JET PTE, to 10.7 MW in TFTR and 16.1 MW in the JET DTE1, while the thermonuclear power gain, defined simply as $Q_{DT} = P_{fus}/P_{aux}$, where P_{aux} is the auxiliary heating power injected into the torus, rose from 0.12 in the JET PTE, to 0.27 in TFTR and 0.62 in the JET DTE1. Figure 6.16 illustrates the pulses which produced the highest fusion powers in each of these experiments.

In almost all of the cases shown, the fusion power pulse lasts for only 1…2 s, a period which is determined by plasma confinement and stability limits. In both TFTR and JET, the plasma regimes with the highest fusion performance were developed from low density target plasmas into which high power (15…40 MW) NBI was injected. This fuels the plasma centrally, raises the central ion temperature to values in the region of 20…40 keV, typically a factor of 2…3 greater than the central electron temperature, and produces a "hot-ion" mode in which energy confinement times can be up to a factor of 4 higher than the L-mode level. In TFTR, a limiter device, the regime is referred to as a "supershot" [87S1], while that in JET is a "hot-ion H-mode" [92J1]. A variation of the scenario, also illustrated in the figure, is based on the use of an "optimized (magnetic) shear" mode, in which an internal transport barrier is exploited to improve the core plasma performance. In all cases, the improvement in confinement can be maintained only transiently, and the plasma fusion performance decays after ≈ 1…2 s, an occurrence which is often triggered by mhd activity. An additional feature of these plasma regimes is that the fast ion slowing down time is relatively long, due to the high central electron temperature, so that beam-plasma and beam-beam reactions contribute a significant fraction, usually above 50 %, of the fusion power. In the plasmas which produced the highest fusion power in JET, however, this non-thermal component amounted to only ≈ 40 %. The contrast with the performance of quasi-steady-state plasma regimes is also illustrated in the figure, as exemplified by an ELMy H-mode which produced the highest fusion energy. Though the fusion power is more modest than for the transient cases, amounting to ≈ 25 % of the highest fusion power and corresponding to $Q_{DT} = 0.18$, the pulse duration was not limited by intrinsic plasma characteristics, but rather by the requirement to limit the overall neutron production in the experiment.

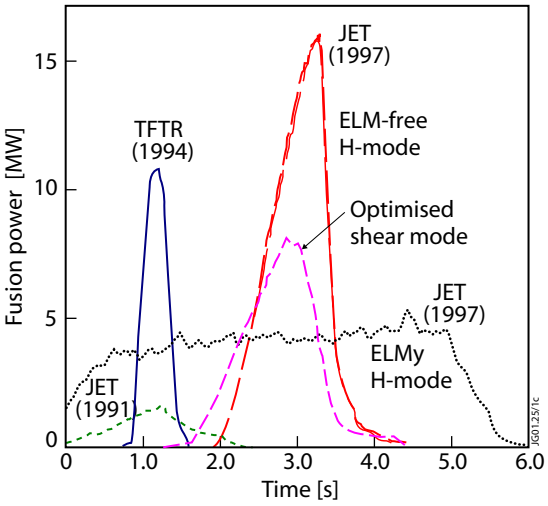

Fig. 6.16. Time histories of the highest fusion power pulses produced in various confinement regimes during the JET and TFTR D-T experiments [99K2].

These experiments provided precise confirmation of the plasma performance predictions which had been made for D-T plasmas on the basis of deuterium experiments. They also yielded key information on the influence of the hydrogen isotope mass on energy confinement, revealing, in particular, that its influence could depend on confinement regime. In TFTR, for example, it was found that the *total* energy confinement time in L-mode discharges was consistent with $\tau_E \propto \langle A \rangle^{0.3-0.5}$, where $\langle A \rangle$ is the volume averaged isotope mass, while in supershot plasmas $\tau_E \propto \langle A \rangle^{0.82}$. JET H-mode experiments, however, indicated that the *thermal* energy confinement time satisfied $\tau_E \propto \langle A \rangle^{0.03\pm0.1}$, a somewhat weaker mass dependence than that given in (6.43). Moreover, by expressing the plasma energy as the sum of two components, one associated with the H-mode edge pedestal, the other identified with the energy confinement of the plasma core (i.e. the region between the magnetic axis and the edge pedestal), it was shown that the core thermal energy confinement time varied as $\langle A \rangle^{-0.16\pm0.1}$, which is in good agreement with the dependence expected if core confinement is determined by so-called "gyro-Bohm" processes (i.e. the underlying turbulence responsible for heat transport has a radial correlation length of $\approx \rho_{iL}$ [99I1]). The JET experiments also confirmed the $\langle A \rangle^{-1}$ dependence of the H-mode power threshold (see (6.41)).

The thermalization and confinement of α-particles were analyzed in some detail. As noted in Sect. 6.8, electron heating due to α-particles was observed at the expected level. The α-particle energy distribution formed as the α-particles slow down was also investigated in TFTR, confirming that the energy distribution, measured over the range 0.1…3.5 MeV, was as expected on the basis of classical slowing down via Coulomb collisions. Analysis of the radial profile of the α-particles indicated that any anomalous diffusion coefficient must be of the same order as the neoclassical diffusion coefficient, i.e. almost two orders of magnitude smaller than the anomalous electron diffusion coefficient observed in equivalent discharges. Studies of the influence of sawteeth and disruptions on the α-population in TFTR showed that while sawteeth could redistribute the α-particles within the plasma in a manner consistent with the occurrence of magnetic reconnection, disruptions produced rapid and substantial losses of α-particles, with up to 20 % of the α's being lost within 2 ms at the thermal quench. In addition, some evidence was obtained in TFTR, under carefully adjusted conditions, for the excitation of TAE modes by the α-population. The detailed observations of α-particle behavior made during these experiments, together with the validation of theoretical models used for extrapolation, provide confidence that in burning plasmas α-particles will be well confined and provide the expected level of plasma heating.

6.10 ITER and tokamak power plants

6.10.1 ITER

The International Thermonuclear Experimental Reactor (ITER) is a long pulse burning plasma experiment which is being designed as the next major step in the international tokamak program through a collaboration between the European Union, Japan and the Russian Federation [01A2, 02I1]. Its principal physics goals are: (1) to achieve extended burn in inductively driven plasmas with a Q_{DT} of at least 10; (2) to aim at demonstrating steady-state operation using non-inductive current drive with a Q_{DT} of at least 5. In addition, under favorable confinement conditions, the device should be capable of studying "controlled ignition", with $Q_{DT} \approx 50$. ITER is also intended to demonstrate the maturity of the magnetic fusion program with respect to key aspects of the technology required for a fusion power plant and has as its central technological goals: (1) to demonstrate the availability and integration of essential fusion technologies; (2) to test components for a future fusion reactor; (3) to test concepts for tritium breeding modules using the 14.1 MeV neutron flux at the first wall. It should, moreover, establish the favorable safety and environmental characteristics of fusion as an energy source. The principal parameters of the design are given in Table 6.3.

Figure 6.17 shows a cutaway view of the ITER device with the main elements of the design indicated. To achieve long plasma pulses, ≥ 300 s at the nominal plasma current of 15 MA, the design uses superconducting toroidal and poloidal field magnet systems. The toroidal field magnet and the central solenoid are fabricated from Nb_3Sn strand, due to the requirement for maximum magnetic fields of ≈ 13 T, while the remainder of the poloidal field coils are fabricated from NbTi strand. The coils are cooled by supercritical helium and operate at a nominal temperature of 4.5 K, so that the entire device must be contained within a cryostat. As illustrated in Fig. 6.18a, a double-walled steel vacuum vessel and 45 cm thick shielding blanket modules provide thermal and neutron shielding for the coils and external components of the tokamak. All major structural elements are fabricated from 316L(N) stainless steel and water is used in all cooling circuits, with a nominal blanket coolant temperature of 400 K, since ITER is not designed to generate electricity. Figure 6.18b, which shows the heat flux arising from the kinetic energy of the fusion neutrons as a function of major radius on the inboard side of the torus, illustrates the degree of shielding provided by the blanket and vacuum vessel: the heat flux at the outer edge of the TF coil inboard leg is a factor of 10^5 below that at the chamber first wall, and the total heat load on the TF coils resulting from a fusion output power of 500 MW is only 13 kW.

A mixture of plasma facing materials is employed: beryllium on the first wall of the main plasma chamber, CFC on the high heat flux components in the divertor and tungsten in the remainder of the divertor. This is designed to minimize contamination of the plasma while providing resistance to erosion in the divertor, where the heat and particle fluxes are highest. The plasma is fueled with a mixture of gas puffing and cryogenic pellet injection, while particle exhaust during plasma operation is provided by a series of cryopumps, located adjacent to the divertor chamber, operating at 4.5 K and coated with activated charcoal for the extraction of helium. An initial auxiliary heating and current drive system consisting of 33 MW of NBI, based on 1 MeV negative ion technology, 20 MW of ICRF, operating in the range 40…55 MHz, and 20 MW of ECRF at 170 GHz is foreseen. Further heating and current drive systems, including LHCD, can be added in the course of the experimental program to provide additional flexibility.

Testing of tritium breeding technology is an important aspect of the ITER program. If required, the shielding blanket could be replaced by a tritium breeding blanket over the outboard half of the vessel surface. The same structural and plasma facing materials would be used as in the shielding blanket and the modules would remain water cooled. However, additional breeding boxes containing a beryllium multiplier in pebble form and a lithium ceramic breeder material (e.g. Li_2ZrO_3, Li_2TiO_3, or Li_4SiO_4) would be incorporated into the modules and helium would be used to purge tritium from the system. Several main horizontal ports have also been reserved to provide operational tests of potential breeding blanket designs for tokamak power plants. Modules based on design concepts discussed in Sect. 6.10.2 will be installed at an early stage of the ITER program to gain experience of their behavior in the tokamak environment and, ultimately, to yield quantitative information on the achievable tritium breeding ratio (i.e. the ratio of tritium atoms produced to neutrons emitted from the plasma).

Table 6.3. Principal parameters of the ITER design.

Toroidal field		5.3 T
Plasma current		15 MA
Major, minor radius		6.2 m, 2.0 m
Aspect ratio		3.1
Elongation (95 % flux)		1.70
Triangularity (95 % flux)		0.33
Safety factor (95 % flux)		3.0
Plasma volume		837 m^3
Fusion power (Q_{DT} = 10):	nominal	500 MW
	range	200…700 MW
Neutron flux at first wall:	nominal	0.57 $MW\,m^{-2}$
Lifetime neutron fluence		0.3 $MW\,a\,m^{-2}$
Plasma inductive burn duration (Q_{DT} = 10)		≥ 300 s
Auxiliary heating and current drive power		73 MW
Nominal Q_{DT}		10
First wall material		beryllium
(Shielding) Blanket material		SS 316 L(N)
Blanket coolant		water (3MPa)
Blanket coolant flow rate		3378 $kg\,s^{-1}$

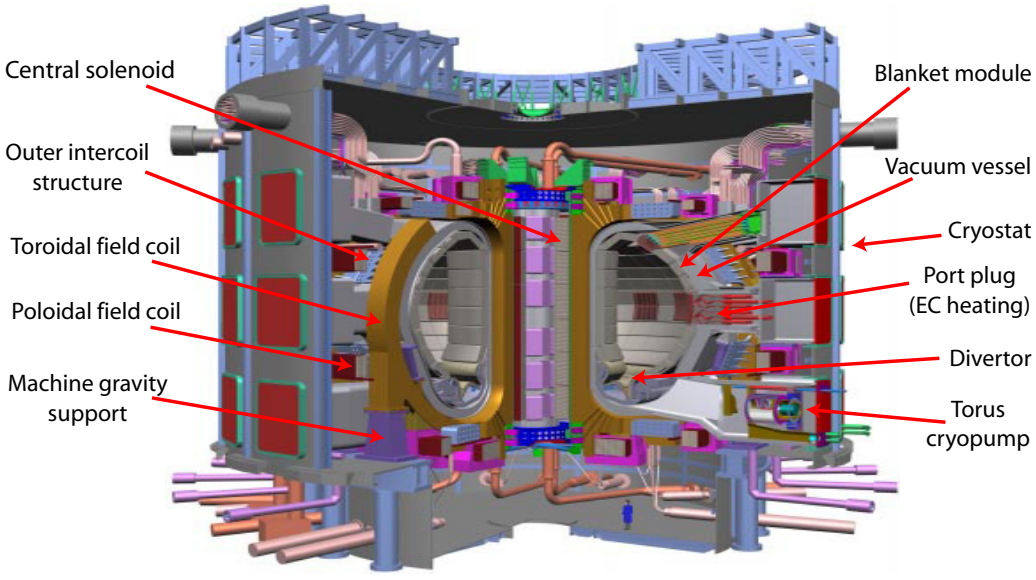

Fig. 6.17. A 3-D cutaway view of the proposed ITER burning plasma experiment showing the main elements of the design [01A2].

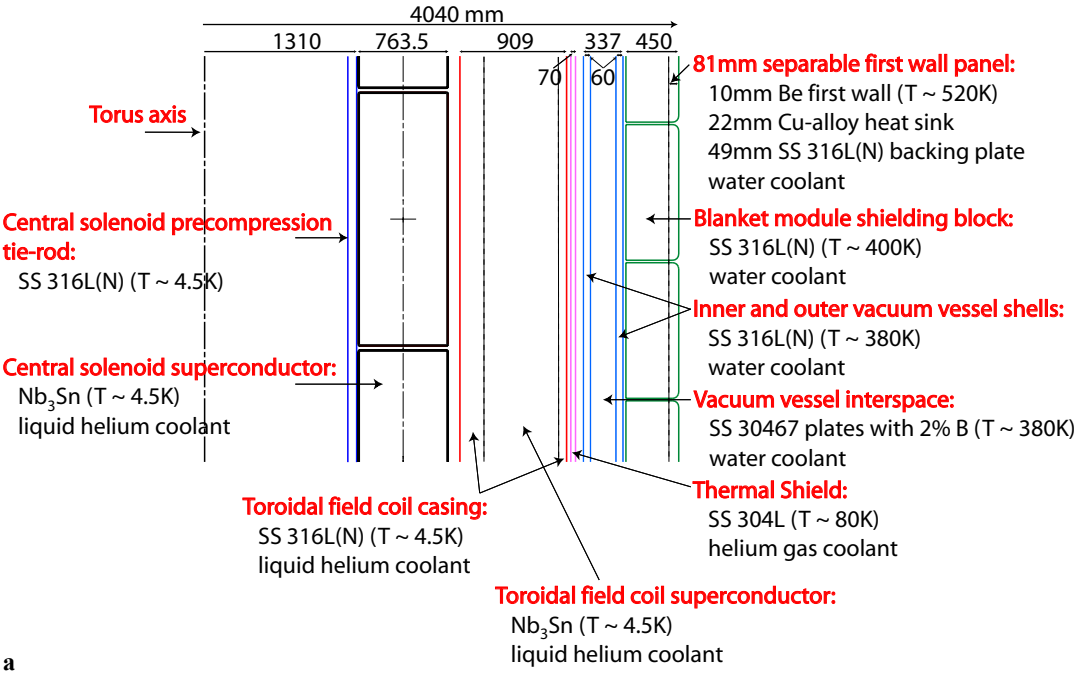

a

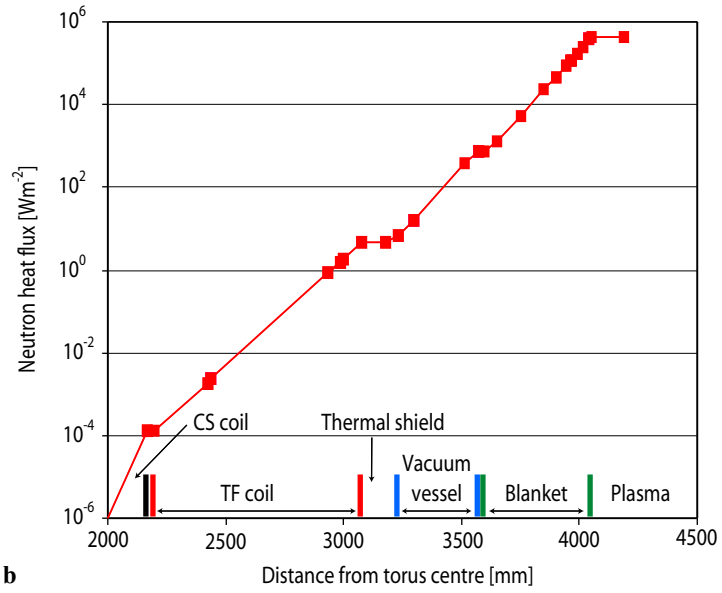

b

Fig. 6.18. **(a)** Cross-section through the equatorial inboard (high magnetic field side) structures of the ITER tokamak, indicating the materials used, the coolant in each structure and the operating temperature in each region. The structural dimensions are given at room temperature. **(b)** Heat flux associated with the neutron kinetic energy through the inboard structures of the ITER tokamak for a plasma operating scenario with 500 MW of fusion power.

In inductive operation, ITER is designed to operate in an ELMy H-mode, which has a demonstrated long-pulse capability, ensuring that the device should achieve an inductive burn duration of at least 300 s. Figure 6.19 illustrates the predicted $Q_{DT} = 10$ operating window for ITER in terms of fusion power and energy confinement enhancement factor relative to the IPB98(y,2) scaling (see (6.43)). The principal limitations to the operating domain are set by the H-mode power threshold, the maximum attainable density and the β-limit, here expressed in terms of the achievable value of β_N. If H-mode confinement can be sustained at densities above the Greenwald value, n_{GW}, or the confinement enhancement factor can be increased to ≈ 1.2, as obtained in some current experiments, or operation at higher current ($I_p \approx 17$ MA, corresponding to $q_{95} \approx 2.6$) can be established without significant confinement degradation, $Q_{DT} \approx 50$ can also be achieved. The inductive mode of operation will allow ITER to address many aspects of burning

plasma physics of relevance to reactor plasmas, including confinement behavior, density and pressure limits, power and particle control, and α-particle physics, on timescales which are long with respect to all of the key timescales for plasma processes to reach equilibrium. Steady-state operation at $Q_{DT} = 5$, which will involve plasma scenarios of the type discussed in Sect. 6.7, will permit candidate regimes for steady-state operation in fusion reactors to be investigated under conditions in which α-particles make a significant contribution to plasma pressure. Fulfillment of this goal will represent a substantial step towards the development of a viable steady-state mode of plasma operation for tokamak power plants.

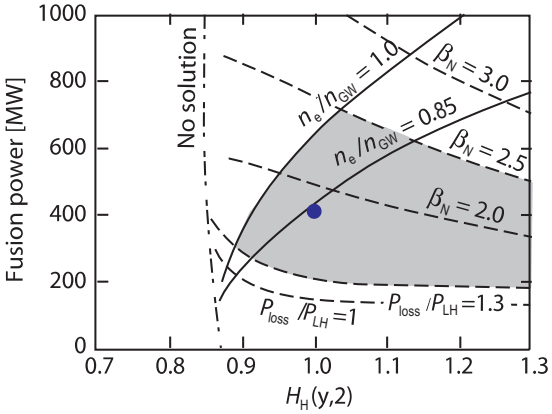

Fig. 6.19. Predicted $Q_{DT} = 10$ operating window for inductive plasmas with $I_p = 15$ MA in ITER in terms of the fusion power and confinement enhancement factor relative to the IPB98(y,2) energy confinement scaling, H_H(y,2). The shaded area indicates the $Q_{DT} = 10$ domain, delimited by boundaries in power flow across the plasma separatrix relative to the H-mode power threshold, $P_{loss}/P_{LH} = 1.3$, plasma density relative to the Greenwald density, $n/n_{GW} = 1.0$, and normalized plasma β, $\beta_N = 2.5$ [01A2].

6.10.2 Tokamak power plants

Extensive studies of the physics and technology characteristics of tokamak power plants based on the deuterium-tritium-lithium fuel cycle have been performed during the last 30 years. These studies have provided guidance to the magnetic fusion program in relation to the key elements of reactor physics and technology which will influence the final cost of electricity (COE), which is likely to have a central bearing on the development of fusion as an economically acceptable energy source. They have also identified critical issues in the areas of operational reliability and availability, environmental cleanliness and safety, which are essential to the commercial success and public acceptance of fusion energy. Early considerations are discussed in [81C1], while the physics basis which has been developed for tokamak power plants is reviewed in [93K1, 94S1, 99I1].

Factors determining the cost of fusion energy are analyzed in [95G2, 96H1, 97W2, 01W1, 01W2], where it is shown that the capital cost of the fusion core, including the replacement of items such as the first wall, blanket and divertor, which will suffer erosion or radiation damage, dominates the COE. The plasma physics quantity having the greatest impact on cost is the attainable β, usually expressed in terms of β_N, which reflects whether the assumptions inherent in a particular design meet existing experimental constraints or require further development. Additional factors contributing to the COE include the choice of pulsed or steady-state operation, with the latter now recognized as having both economic and engineering advantages (e.g. [94B3, 95G2]), plant availability, thermodynamic efficiency and the power plant unit size: COE typically decreases with increasing unit size, although studies have in the main settled on a unit size of ≈ 1000 MW electrical as the largest unit which will be acceptable to electricity utilities. A further significant influence on COE derives from the cost advantage which can be obtained as a result of series production, with cost reductions in the range of 20…50 % assumed for a "tenth of a kind" power plant (e.g. [96H1]). The COE target for fusion energy, which may not be deployed for 50 years, is fraught with uncertainties, but as an indication, the ARIES studies (e.g. [97N3]) aimed at a COE in the range 6.5…8 US cents/kWh.

Table 6.4 illustrates the principal parameters of several recent power plant studies and demonstrates how assumptions made in relation to physics and technology influence the scale (and, by implication, cost) of the resultant devices. In particular, the ARIES-RS and A-SSTR2 designs illustrate the application of the latest concept in "conventional", i.e. moderate to high aspect ratio, tokamak designs in which ad-

vanced tokamak scenarios (as discussed in Sect. 6.7) are exploited to produce high-β_N compact devices capable of steady-state operation. However, they differ significantly in relation to the technology exploited, for example in the TF magnet design: ARIES-RS utilizes conventional Nb_3Sn strand for the TF conductor, while the A-SSTR2 designers propose a high-temperature superconducting strand made from Bi-Ag alloy, operating at 20 K and allowing a substantially higher field (23 T) at the TF coil inner leg. A-SSTR2 also dispenses entirely with a central solenoid, relying on non-inductive current drive for the current ramp-up, uses a helium cooled SiC/SiC composite design for the blanket module, and relies on the beneficial scaling of COE with unit size, producing 2550 MW of electrical power.

In contrast to these devices, the SEAFP study demonstrates the scale of device required to achieve an electrical power output of 1000 MW using conventional ELMy H-mode physics constraints to obtain steady-state operation, while the PULSAR-I study is illustrative of a pulsed reactor design, but one which exploits certain elements of advanced physics. The final device, STPP, is based on the spherical tokamak concept (Sect. 6.9.1) and so uses a water-cooled copper TF magnet system, in contrast to the superconducting TF coils of the other designs. Though having the smallest major radius of the designs shown, the plasma volume is approximately a factor of 3 larger than e.g. the ARIES-RS design, so that it is not the most compact device, and, due to the water-cooled TF coil, it has a significantly higher recirculating power fraction, which has a considerable impact on the design optimization.

To obtain "acceptable" COE and/or operating characteristics, power plant designs must typically assume that the optimum parameters achieved in existing experiments, or predicted on theoretical grounds, can be realized at the reactor scale. This is not unreasonable, since it will require approximately 50 years of R&D, at current levels of resources, until the commissioning of a prototype commercial reactor. These assumptions serve, moreover, to highlight the key R&D areas for the future. Principal amongst these assumptions is that $\beta_N \approx 4\ldots5$ (conventional aspect ratio), or ≈ 8 (low aspect ratio), can be attained, implying that techniques for active control of mhd stability are available. Achievement of such β_N values generally involves energy confinement beyond normal ELMy H-mode levels, though the values required ($H_H(y,2) = 1.5$ is common) are not exceptional in comparison to those achieved in transient conditions in existing experiments. Nevertheless, an advanced tokamak scenario will probably be required to sustain this level of β_N and confinement enhancement in steady-state.

Fully non-inductive current drive is essential for steady-state operation. In order to minimize the recirculating electrical power required for auxiliary current drive systems, conventional aspect ratio designs generate 80…90 % of the plasma current via the bootstrap effect, while low aspect ratio power plants seek to achieve pressure driven current fractions of at least 90 %. These bootstrap fractions are consistent with the β_N values proposed, but external current drive systems must provide the remainder of the current at high current drive efficiencies while controlling the current profile to maintain mhd stability. Maintaining satisfactory divertor operation, in particular, constraining the exhaust power flux to the divertor targets to values below $\approx 10\ MWm^{-2}$, set by technological constraints, is a major challenge. Recent designs rely on tungsten as the principal power handling material, so that divertor plasma temperatures below ≈ 20 eV are required to limit core plasma contamination [95W1]. The solution generally advanced is a development of the power dissipation scenario proposed for ITER, in which low concentrations ($\approx 1\ldots2$ %) of impurities such as neon or argon are introduced to radiate most (perhaps 80 %) of the exhaust power to the first wall. The fundamental challenge of power exhaust is not significantly affected by the choice of SNX or DNX plasma configurations. Disruptions interrupt the routine operation of a power plant and represent a threat to the integrity of the reactor first wall. It is expected, therefore, that the disruption frequency in tokamak power plants should fall to $0.1\ldots1\ a^{-1}$, compared to an observed frequency of up to 10 % of plasma pulses in present devices. This will necessitate an extensive R&D program to improve the ability to recognize plasma conditions leading to disruptions and to allow plasma parameters to be actively adjusted to maintain the plasma inside the stable region.

Table 6.4. Principal parameters of several recent tokamak power plant studies.

Parameter		SEAFP [95R1]	PULSAR-I [94B3]	ARIES-RS [97N3]	A-SSTR2 [01N1]	STPP [00A1]
Toroidal field (axis)	[T]	7.8	6.7	8.0	11	1.8
Plasma current	[MA]	10.4	14.2	11.3	12	31
Major, minor radius	[m]	9.4, 2.1	9.2, 2.3	5.52, 1.38	6.2, 1.5	3.42, 2.44
Aspect ratio		4.5	4.0	4.0	4.1	1.4
Elongation (95 % flux)		1.66	1.6	1.7	1.8	3.0
Triangularity (95 % flux)		0.2	0.35	0.5	0.4	0.45
Safety factor (95 % flux)		3.9	3.5	3.5	5.2	10.8
Plasma volume	[m^3]	1360	1540	350	470	1081
Auxiliary power	[MW]	75	0	81	85	76
Fusion power	[MW]	3000	2030	2170	4000	3300
Total thermal power [1])	[MW]	3500	2310	2620	5000	4090
Net electrical power	[MW]	1000	1000	1000	2550	1214
Av. neutron wall load	[$MW\,m^{-2}$]	2.1	1.1	4.0	6.0	3.7
Operation mode		steady-state	2.5 h pulse	steady-state	steady-state	steady-state
τ_E	[s]	2.2	3.8	1.34	1.4	1.8
β, β_N		2.2 %, 3.5	2.8 %, 3.0	5 %, 5.0	2.9 %, 4.0	58 %, 8.2
$<n_e>$	[$10^{20}\,m^{-3}$]	1.6	1.2	2.1	2.0	1.39
$<T_e>$	[keV]	10	15	18.7	21	16.9
First wall material		Be or W		V-alloy		C
First wall structure		(i) V5Ti (ii) f-m SS [5])	SiC/SiC	V-alloy	SiC/SiC	f-m SS [5])
First wall coolant		(i) He (ii) water	He	liquid Li	He	He
Breeding blanket structure		(i) V5Ti (ii) f-m SS [5])	SiC/SiC	V-alloy	SiC/SiC	f-m SS [5])
Breeding material [2])		(i) Li_2O (ii) $Li_{17}Pb_{83}$	Li_2O	liquid Li	Li_2TiO_3	Li_2O
Breeding blanket coolant temperature [3])	[K]	(i) 830 (ii) 580	< 1200	880	1170	720
Breeding blanket coolant		(i) He (ii) water	He	liquid Li	He	He
Shield blanket material		a SS [6])	SiC/SiC	(i) V-alloy [4]) (ii) SS	TiH_2	f-m SS [5])
Vacuum. vessel structure		a SS [6])		SS		f-m SS [5])

[1]) Total thermal power exceeds the fusion power due to the exothermic tritium-breeding reactions.

[2]) Li_2O and Li-ceramic (e.g. Li_2TiO_3) breeder materials generally require a neutron multiplier (e.g. Be) and enrichment (≈30…60 %) of ^6Li (7.5 % content in natural lithium).

[3]) Outlet temperature of coolant – temperature of breeder material may be higher.

[4]) V-alloy used in high temperature section of shield and stainless steel in low temperature section.

[5]) f-m SS: ferritic-martensitic stainless steel.

[6]) a SS: austenitic stainless steel.

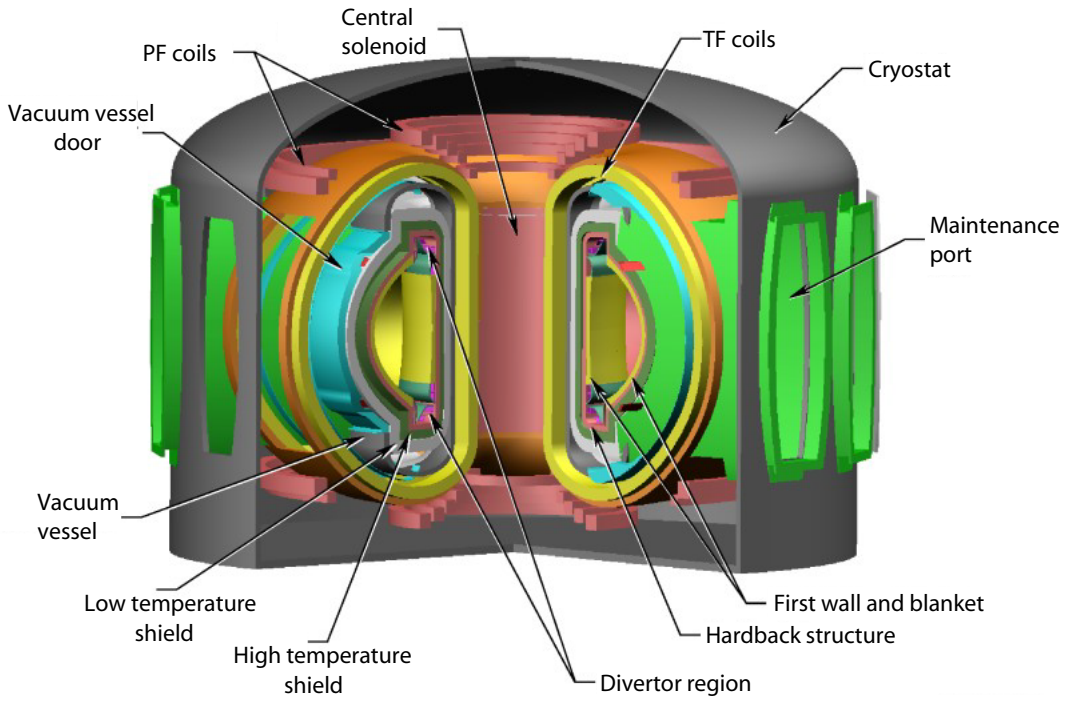

Fig. 6.20. A 3-D cutaway view of the fusion core of the ARIES-RS power plant study [97N3].

Figure 6.20 shows a 3-D cutaway view of the fusion core of the ARIES-RS design. Although it is very similar, topologically, to the ITER design illustrated in Fig. 6.17, there are significant technological differences between the two devices which are representative of the advances which the tokamak program must make in progressing from a Next Step burning plasma experiment to a power plant. Moving out from the center of the plasma, plasma facing materials, particularly in high heat flux areas such as the divertor, will probably be based on high-Z materials, such as tungsten, to maximize their lifetime and to avoid problems with tritium retention via codeposition. The next major component, the blanket modules, will be considerably different from those in a Next Step device, where the principal function is to provide neutron shielding. Reactor blanket modules must provide high grade heat for electricity generation, which implies operation at temperatures of up to 1200 K in some designs, and probably necessitates the use of coolants such as helium or liquid metals, rather than water. The blanket modules must also breed tritium efficiently via the reactions of neutrons with lithium, implying the use of lithium ceramics or liquid metal as a breeder, and probably also necessitating the incorporation of beryllium or lead as a neutron multiplier (e.g. [00G2]). To exploit the environmental attractiveness of fusion energy fully, all structural materials in the fusion core will need to consist of low activation materials, such as certain ferritic-martensitic steels currently under development, or more speculatively vanadium or SiC/SiC composites (e.g. [92R1, 99E1]). Since average neutron wall loads are expected to lie in the range 2…6 $MW\,m^{-2}$, these materials must also be resistant to neutron damage to minimize the loss of plant operating time associated with replacement of the blanket modules (and high heat flux components). Situated behind the blanket module is a metallic shield which is ≈ 0.5…1 m thick and which is designed to further reduce the neutron flux, by a factor of at least 10^4, to ensure the survival of the superconducting coils for the life of the plant.

While the superconducting materials proposed for the ITER magnet systems, Nb_3Sn for the central solenoid and toroidal field coils and NbTi for the poloidal field coils, feature in many power plant designs, advanced high temperature superconductors, such as the Bi-Ag alloy proposed for A-SSTR2, if successfully developed, could permit more compact and cheaper power plants. For low aspect ratio designs, however, a superconducting TF magnet system is not viable, so approaches such as water-cooled copper operating at room temperature and helium-cooled aluminium operating at ≈ 30 K are under investigation [00V1]. Auxiliary systems, such as heating and current drive, fueling and pumping, and diagnostic (i.e.

control) systems, will probably evolve naturally from systems applied at the ITER scale, but they will require performance developments beyond those required for ITER to function continuously in the demanding environment of a power plant. Steady-state operation will require, in particular, that these systems are effectively and reliably coupled to provide the requisite degree of control of the plasma operating point. Outside of the fusion core, a power plant must have an efficient tritium extraction and reprocessing plant to ensure that tritium exhausted from the plasma and bred in the blanket can be processed on acceptable timescales to minimize the on-site tritium inventory. The physics and technology developments required by the tokamak fusion program to proceed to the construction of a fusion power plant are discussed in [92M1, 99N1, 00A2, 02L1].

6.11 References for 6

53S1 Spitzer, L., Härm, R.: Phys. Rev. **89** (1953) 977.
66S1 Shafranov, V.D.: in Reviews of Plasma Physics, Leontovich, M.A. ed., Vol. 2, Consultants Bureau, New York (1966).
69P1 Peacock, N.J. et al.: Nature **224** (1969) 488.
70B1 Kadomtsev, B.B., Pogutse, O.P.: in Reviews of Plasma Physics, Leontovich, M.A. ed., Vol. 5, Consultants Bureau, New York (1970).
70O1 Ohkawa, T.: Nucl. Fusion **10** (1970) 185.
71B1 Bickerton, R.J. et al.: Nat. Phys. Sci. **229** (1971) 110.
72S1 Stix, T.H.: Plasma Phys. **14** (1972) 367.
74V1 von Goeler, S. et al.: Phys. Rev. Lett. **33** (1974) 1201.
75S1 Stix, T.H.: Nucl. Fusion **15** (1975) 737.
76H1 Hinton, F.L., Hazeltine, R.D.: Rev. Mod. Phys. **48** (1976) 239.
77H1 Hirschman, S.P. et al.: Nucl. Fusion **17** (1977) 611.
78B1 Bateman, G.: MHD Instabilities, MIT Press, Cambridge, Mass. (1978).
79G1 Galeev, A.A., Sagdeev, R.Z.: in Reviews of Plasma Physics, Leontovich, M.A. ed., Vol. 7, Consultants Bureau, New York (1979).
81C1 Conn, R.W.: Chap. 14 of Fusion, Vol. 1B, Teller, E. ed., Academic Press, New York (1981).
81G1 Greene, J.M., Chance, M.S.: Nucl. Fusion **21** (1981) 453.
81H1 Hirschman, S.P., Sigmar, D.J.: Nucl. Fusion **21** (1981) 1079.
81H2 Hemsworth, R.S.: Chap. 20 of Plasma Physics and Nuclear Fusion Research, Gill, R.D. ed., Academic Press, London (1981).
81S1 Stringer, T.E.: Comp. Phys. Commun. **24** (1981) 337.
82W1 Wagner, F. et al.: Phys. Rev. Lett. **49** (1982) 1408.
83B1 Bornatici, M. et al.: Nucl. Fusion **23** (1983) 1153.
83M1 McGuire, K. et al.: Phys. Rev. Lett. **50** (1983) 891.
84G1 Goldston, R.J.: Plasma Phys. Control. Fusion **26(1A)** (1984) 87.
84L1 Lipschultz, B. et al.: Nucl. Fusion **24** (1984) 977.
84T1 Troyon, F. et al.: Plasma Phys. Control. Fusion **26(1A)** (1984) 209.
86C1 Cheng, C.Z., Chance, M.S.: Phys. Fluids **26** (1986) 3695.
86P1 Peng, Y.K.M., Strickler, D.J.: Nucl. Fusion **26** (1986) 769.
87F1 Fisch, N.J.: Rev. Mod. Phys. **59** (1987) 175.
87F2 Freidberg, J.P.: Ideal Magnetohydrodynamics, Plenum Press, New York (1987).
87H1 Hutchinson, I.H.: Principles of Plasma Diagnostics, Cambridge University Press, Cambridge (1987).
87S1 Strachan, J.D. et al.: Phys. Rev. Lett. **58** (1987) 1004.
88C1 Campbell, D.J. et al.: Nucl. Fusion **28** (1988) 981.
88C2 Campbell, D.J. et al.: Phys. Rev. Lett. **60** (1988) 2148.
88G1 Greenwald, M. et al.: Nucl. Fusion **28** (1988) 2199.
88O1 Orlinskij, D.V., Magyar, G.: Nucl. Fusion **28** (1988) 611.

88Z1 Zarnstorff, M.C. et al.: Phys. Rev. Lett. **60** (1988) 1306.
89F1 Fu, G.Y., Van Dam, J.W.: Phys. Fluids **B1** (1989) 1949.
89M1 Miyamoto, K.: Plasma Physics for Nuclear Fusion, revised edition, MIT Press, Cambridge, Mass. (1989).
89W1 Wesson, J.A. et al.: Nucl. Fusion **29** (1989) 641.
90K1 Kikuchi, M. et al.: Nucl. Fusion **30** (1990) 343.
90L1 Lister, J.B. et al.: Nucl. Fusion **30** (1990) 2349.
90R1 Reiter, D. et al.: Nucl. Fusion **30** (1990) 2141.
90S1 Stangeby, P.C., McCracken, G.M.: Nucl. Fusion **30** (1990) 1225.
90Y1 Yushmanov, P.N. et al.: Nucl. Fusion **30** (1990) 1999.
90Z1 Zarnstorff, M.C. et al.: Phys. Fluids **B2** (1990) 1852.
91C1 Cairns, R.A.: Radiofrequency Heating of Plasmas, Adam Hilger, Bristol (1991).
91H1 Heidbrink, W.W. et al.: Nucl. Fusion **31** (1991) 1635.
91J1 Jackson, G.L. et al.: Phys. Rev. Lett. **67** (1991) 3098.
91P1 Post, D.E. et al.: ITER Physics, ITER Documentation Series No. 21, IAEA, Vienna (1991).
91S1 Stork, D.: Fusion Eng. Des. **14** (1991) 111.
91T1 Tubbing, B.J.D. et al.: Nucl. Fusion **31** (1991) 839.
91W1 Wong, K.L.: Phys. Rev. Lett. **66** (1991) 1874.
92J1 The JET Team: Nucl. Fusion **32** (1992) 187.
92K1 Kadomtsev, B.B.: Tokamak Plasma: A Complex Physical System, Institute of Physics Publishing, Bristol (1992).
92L1 Lao, L.L. et al.: Phys. Fluids **B4** (1992) 232.
92M1 Mizoguchi, T.: Fusion Eng. Des. **15** (1992) 361.
92R1 Rocco, P., Zucchetti, M.: Fusion Eng. Des. **15** (1992) 235.
92S1 Stix, T.H.: Waves in Plasmas, American Institute of Physics, New York (1992).
93G1 Gruber, O. et al.: Plasma Phys. Control. Fusion **35** (1993) B191.
93K1 Kikuchi, M.: Plasma Phys. Control. Fusion **35** (1993) B39.
93T1 Todd, T.N.: Chap. 17 of Plasma Physics: An Introductory Course, Dendy, R.O. ed., Cambridge University Press, Cambridge (1993).
94B1 Burrell, K.H. et al.: Phys. Plasmas **1** (1994) 1536.
94B2 Bondeson, A., Ward, D.J.: Phys. Rev. Lett. **72** (1994) 2709.
94B3 Bathke, C.G. et al.: Fusion Technol. **26** (1994) 1163.
94C1 Connor, J.W., Wilson, H.R.: Plasma Phys. Control. Fusion **36** (1994) 719.
94E1 Erckmann, V., Gasparino, U.: Plasma Phys. Control. Fusion **36** (1994) 1869.
94G1 Goldston, R.J. et al.: Plasma Phys. Control. Fusion **36** (1994) B213.
94H1 Heidbrink, W.W., Sadler, G.J.: Nucl. Fusion **34** (1994) 535.
94K1 Kessel, C. et al.: Phys. Rev. Lett. **72** (1994) 1212.
94R1 Raman, R. et al.: Phys. Rev. Lett. **73** (1994) 3101.
94S1 Sheffield, J.: Rev. Mod. Phys. **66** (1994) 1015.
94S2 Strait, E.J.: Phys. Plasmas **1** (1994) 1415.
95C1 Chang, Z. et al.: Phys. Rev. Lett. **74** (1995) 4663.
95G1 Gruber, O. et al.: Phys. Rev. Lett. **74** (1995) 4217.
95G2 Galambos, J.D. et al.: Nucl. Fusion **35** (1995) 551.
95I1 Ikeda, Y. et al.: Plasma Physics and Controlled Nuclear Fusion Research 1994 (Proc. 15th Int. Conf., Seville, 1994) Vol. 1, IAEA, Vienna (1995) 415.
95K1 Kikuchi, M., Azumi, M.: Plasma Phys. Control. Fusion **37** (1995) 1215.
95L1 Levinton, F.M. et al.: Phys. Rev. Lett. **75** (1995) 4417.
95L2 LaBombard, B. et al.: Phys. Plasmas **2** (1995) 2242.
95M1 Milora, S.L. et al.: Nucl. Fusion **35** (1995) 657.
95R1 Raeder, J. et al.: Safety and Environmental Assessment of Fusion Power (SEAFP), Report EURFUBRU XII-217/95, European Commission, Brussels (1995).

95S1 Söldner, F.X. et al.: Plasma Physics and Controlled Nuclear Fusion Research 1994 (Proc. 15th Int. Conf., Seville, 1994) Vol. 1, IAEA, Vienna (1995) 423.
95S2 Strait, E.J. et al.: Phys. Rev. Lett. **75** (1995) 4421.
95S3 Schüller, F.C. et al.: Plasma Phys. Control. Fusion **37** (1995) A135.
95S4 Strait, E.J. et al.: Phys. Rev. Lett. **74** (1995) 2483.
95T1 Turnbull, A.D. et al.: Phys. Rev. Lett. **74** (1995) 718.
95W1 Wu, C.H., Mszanowski, U.: J. Nucl. Mater. **218** (1995) 293.
96B1 Bécoulet, A.: Plasma Phys. Control. Fusion **38** (1996) A1.
96F1 Fitzpatrick, R., Jensen, T.H.: Phys. Plasmas **3** (1996) 2641.
96G1 Ghendrih, Ph. et al.: Plasma Phys. Control. Fusion **38** (1996) 1653.
96H1 Hender, T.C. et al.: Fusion Technol. **30** (1996) 1605.
96L1 Litaudon, X. et al.: Plasma Phys. Control. Fusion **38** (1996) 1603.
96M1 Messiaen, A. et al.: Phys. Rev. Lett. **77** (1996) 2487.
96P1 Porcelli, F. et al.: Plasma Phys. Control. Fusion **38** (1996) 2163.
96T1 Taylor, G. et al.: Phys. Rev. Lett. **76** (1996) 2722.
96Z1 Zohm, H.: Plasma Phys. Control. Fusion **38** (1996) 105.
97B1 Baylor, L.R. et al.: Nucl. Fusion **37** (1997) 445.
97B2 Bosch, H.S. et al.: J. Nucl. Mater. **241-243** (1997) 82.
97C1 Campbell, D.J. et al.: J. Nucl. Mater. **241-243** (1997) 379.
97F1 Finken, K.H., Wolf, G.H.: Fusion Eng. Des. **37** (1997) 337.
97H1 Hogan, J.: J. Nucl. Mater. **241-243** (1997) 68.
97I1 Itoh, S. et al.: Fusion Energy 1996 (Proc. 16th Int. Conf., Montréal, 1996) Vol. 3, IAEA, Vienna (1997) 351.
97L1 Lang, P. et al.: Phys. Rev. Lett. **79** (1997) 1487.
97M1 Matthews, G.F. et al.: J. Nucl. Mater. **241-243** (1997) 450.
97M2 Miller, R.L. et al.: Phys. Plasmas **4** (1997) 1062.
97N1 Neu, R. et al.: J. Nucl. Mater. **241-243** (1997) 678.
97N2 Najmabadi, F. et al.: Fusion Energy 1996 (Proc. 16th Int. Conf., Montréal, 1996) Vol. 3, IAEA, Vienna (1997) 383.
97N3 Najmabadi, F. et al.: Fusion Eng. Des. **38** (1997) 3.
97P1 Pitcher, C.S., Stangeby, P.C.: Plasma Phys. Control. Fusion **39** (1997) 779.
97P2 Pacher, H.D. et al.: J. Nucl. Mater. **241-243** (1997) 255.
97R1 Rosenbluth, M.N., Putvinski, S.V.: Nucl. Fusion **37** (1997) 1355.
97S1 Sykes, A. et al.: Plasma Phys. Control. Fusion **39** (1997) B247.
97S2 Sauter, O. et al.: Phys. Plasmas **4** (1997) 1654.
97S3 Skinner, C.H. et al.: J. Nucl. Mater. **241-243** (1997) 214.
97S4 Saoutic, B. et al.: Fusion Energy 1996 (Proc. 16th Int. Conf., Montréal, 1996) Vol. 1, IAEA, Vienna (1997) 141.
97T1 Taylor, T.S.: Plasma Phys. Control. Fusion **39** (1997) B47.
97W1 Wesson, J.A.: Tokamaks, second edition, Oxford University Press, Oxford (1997).
97W2 Wootton, A.J. et al.: Nucl. Fusion **37** (1997) 927.
98C1 Connor, J.W.: Plasma Phys. Control. Fusion **40** (1998) 531.
98G1 Gibson, A. et al.: Phys. Plasmas **5** (1998) 1839.
98G2 Garin, P.: Fusion Technology 1998 (Proc. 20th Int. Symp., Marseille, 1998) Vol. 2, CEA, Cadarache (1998) 1709.
98H1 Hofmann, F. et al.: Phys. Rev. Lett. **81** (1998) 2918.
98H2 Hawryluk, R.J.: Rev. Mod. Phys. **70** (1998) 537.
98I1 Technical Basis for the ITER Final Design Report, Cost Review and Safety Analysis (FDR), ITER EDA Documentation Series No. 16, IAEA, Vienna (1998).
98S1 Stott, P.E., Gorini, G., Prandoni, P., Sindoni, E. (eds): Diagnostics for Experimental Thermonuclear Fusion Reactors 2, Plenum Press, New York (1998).

98T1 Tran, M.Q.: Plasma Phys. Control. Fusion **40** (1998) A53.
98T2 Thomas, P.R. et al.: Phys. Rev. Lett. **80** (1998) 5548.
99E1 Ehrlich, K.: Phil. Trans. R. Soc. Lond. **A357** (1999) 595.
99G1 Giruzzi, G. et al.: Radio Frequency Power in Plasmas (Proc. 13th Topical Conf., Annapolis, 1999) AIP, New York (1999) 35.
99G2 Garofalo, A.M. et al.: Phys. Rev. Lett. **82** (1999) 3811.
99G3 Gruber, O. et al.: Phys. Rev. Lett. **83** (1999) 1787.
99I1 ITER Physics Expert Groups et al.: Nucl. Fusion **39** (1999) 2137.
99J1 Jacquinot, J. et al.: Nucl. Fusion **39** (1999) 235.
99K1 Keilhacker, M. et al.: Nucl. Fusion **39** (1999) 209.
99K2 Keilhacker, M. et al.: Plasma Phys. Control. Fusion **41** (1999) B1.
99M1 Moreau, D., Voitsekhovitch, I.: Nucl. Fusion **39** (1999) 685.
99N1 Najmabadi, F.: Phil. Trans. R. Soc. Lond. **A357** (1999) 625.
99S1 Saibene, G. et al.: Nucl. Fusion **39** (1999) 1133.
99W1 Wong, K.L.: Plasma Phys. Control. Fusion **41** (1999) R1.
00A1 Akers, R.J. et al.: Nucl. Fusion **40** (2000) 1223.
00A2 Andreani, R.: Nucl. Fusion **40** (2000) 1033.
00G1 Gantenbein, G. et al.: Phys. Rev. Lett. **85** (2000) 1242.
00G2 Giancarli, L. et al.: Fusion Eng. Des. **49-50** (2000) 445.
00J1 Jardin, S.C.: Nucl. Fusion **40** (2000) 1101.
00L1 Lister, J.B. et al.: Nucl. Fusion **40** (2000) 1167.
00O1 Oikawa, T. et al.: Nucl. Fusion **40** (2000) 1125.
00S1 Snipes, J.A. et al.: Plasma Phys. Control. Fusion **42** (2000) A299.
00S2 Stangeby, P.C.: The Plasma Boundary of Magnetic Fusion Devices, Institute of Physics Publishing, Bristol (2000).
00V1 Voss, G.M. et al.: Fusion Eng. Des. **48** (2000) 407.
01A1 Allen, S.L. et al.: Fusion Energy 2000 (Proc. 18th Int. Conf., Sorrento, 2000) IAEA, Vienna (2001) paper OV1/3.
01A2 Aymar, R. et al.: Fusion Energy 2000 (Proc. 18th Int. Conf., Sorrento, 2000) IAEA, Vienna (2001) paper OV/1.
01L1 Loarte, A.: Plasma Phys. Control. Fusion **43** (2001) R183.
01N1 Nishio, S. et al.: Fusion Energy 2000 (Proc. 18th Int. Conf., Sorrento, 2000) IAEA, Vienna (2001) paper FTP2/14.
01W1 Ward, D.J. et al.: Fusion Energy 2000 (Proc. 18th Int. Conf., Sorrento, 2000) IAEA, Vienna (2001) paper FTP2/20.
01W2 Wong, C.P.C. et al.: Fusion Energy 2000 (Proc. 18th Int. Conf., Sorrento, 2000) IAEA, Vienna (2001) paper FTP2/17.
02I1 ITER Technical Basis, ITER EDA Documentation Series No. 24, IAEA, Vienna (2002).
02L1 Lackner, K. et al.: J. Nucl. Mater. **307-311** (2002) 10.